Cell Reports

Article

TERRA stability is regulated by RALY and polyadenylation in a telomere-specific manner

Graphical abstract

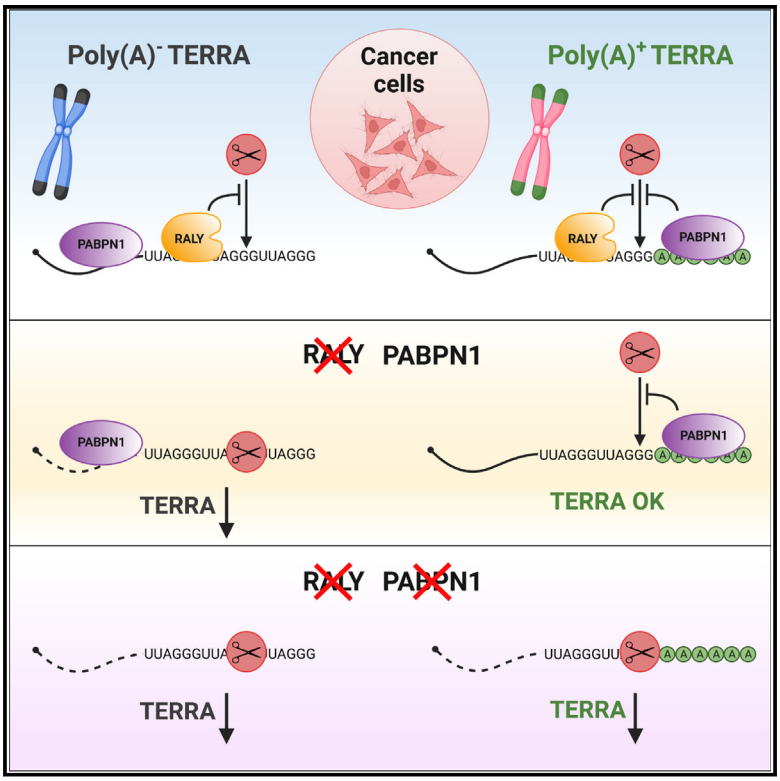

Highlights

- Telomeric RNAs TERRA are polyadenylated in a telomere-specific manner
- TERRA transcripts are bound by the RNA-binding proteins RALY and PABPN1
- RALY stabilizes non-polyadenylated TERRA molecules
- PABPN1 and RALY act redundantly in preserving polyadenylated TERRA stability

Authors

Valeria Savoca, Julieta Rivosecchi, Alice Gaiatto, ..., Toma Tebaldi, Paolo Macchi, Emilio Cusanelli

Correspondence

paolo.macchi@unitn.it (P.M.), emilio.cusanelli@unitn.it (E.C.)

In brief

In this study, Savoca et al. report that human TERRA transcripts are polyadenylated in a telomere-specific manner. TERRA stability is regulated by the concerted action of RALY and PABPN1, which bind both poly(A)$^-$ and poly(A)$^+$ TERRA molecules and regulate their stability in a telomere-specific manner.

Savoca et al., 2023, Cell Reports *42*, 112406
April 25, 2023
https://doi.org/10.1016/j.celrep.2023.112406

CellPress

Cell Reports

CellPress
OPEN ACCESS

Article

TERRA stability is regulated by RALY and polyadenylation in a telomere-specific manner

Valeria Savoca,[1,8] Julieta Rivosecchi,[1,8] Alice Gaiatto,[1,5] Annalisa Rossi,[2] Riccardo Mosca,[1,6] Irene Gialdini,[1,7] Lorena Zubovic,[2] Toma Tebaldi,[3,4] Paolo Macchi,[2,*] and Emilio Cusanelli[1,9,*]

[1]Laboratory of Cell Biology and Molecular Genetics, Department of Cellular, Computational and Integrative Biology - CIBIO, University of Trento, via Sommarive 9, 38123 Trento, Povo, Italy

[2]Laboratory of Molecular and Cellular Neurobiology, Department of Cellular, Computational and Integrative Biology - CIBIO, University of Trento, via Sommarive 9, 38123 Trento, Povo, Italy

[3]Laboratory of RNA and Disease Data Science, Department of Cellular, Computational and Integrative Biology - CIBIO, University of Trento, via Sommarive 9, 38123 Trento, Povo, Italy

[4]Section of Hematology, Department of Internal Medicine, Yale Comprehensive Cancer Center, Yale University School of Medicine, New Haven, CT, USA

[5]Present address: EMBL Heidelberg, Heidelberg, Germany

[6]Present address: Karolinska Institute, Stockholm, Sweden

[7]Present address: Ludwig-Maximilians University of Munich, Munich, Germany

[8]These authors contributed equally

[9]Lead contact

*Correspondence: paolo.macchi@unitn.it (P.M.), emilio.cusanelli@unitn.it (E.C.)

https://doi.org/10.1016/j.celrep.2023.112406

SUMMARY

Telomeric repeat-containing RNA (TERRA) is a long non-coding RNA transcribed from telomeres that plays key roles in telomere maintenance. A fraction of TERRA is polyadenylated, and the presence of the poly(A) tail influences TERRA localization and stability. However, the mechanisms of TERRA biogenesis remain mostly elusive. Here, we show that the stability of TERRA transcripts is regulated by the RNA-binding protein associated with lethal yellow mutation (RALY). RALY depletion results in lower TERRA levels, impaired localization of TERRA at telomeres, and ultimately telomere damage. Importantly, we show that TERRA polyadenylation is telomere specific and that RALY preferentially stabilizes non-polyadenylated TERRA transcripts. Finally, we report that TERRA interacts with the poly(A)-binding protein nuclear 1 (PABPN1). Altogether, our results indicate that TERRA stability is regulated by the interplay between RALY and PABPN1, defined by the TERRA polyadenylation state. Our findings also suggest that different telomeres may trigger distinct TERRA-mediated responses.

INTRODUCTION

Telomeric repeat-containing RNA (TERRA) is a class of long non-coding RNAs transcribed from chromosome ends in a variety of organisms.[1–5] TERRA transcription relies on RNA polymerase II and initiates within subtelomeric regions to proceed toward the end of the chromosomes, terminating within the telomeric repeat tract.[6] As a consequence, the 5′ end of TERRA contains chromosome-specific subtelomeric sequences, while the 3′ extremity of TERRA transcripts consists of G-rich telomeric sequences ($UUAGGG_n$ in vertebrates).[7] In humans, TERRA promoter regions have been identified at CpG di-nucleotide-rich DNA islands located in proximity of the telomeric tract in about half of chromosomes[8] and at 5–10 kb from the telomeric tract in 10 different chromosomes.[9]

Intriguingly, despite the absence of polyadenylation sites within the telomeric sequences, 7% of the total population of TERRA is polyadenylated in human cells.[10] Polyadenylated TERRA molecules localize within the nucleoplasm, while the non-polyadenylated transcripts are found both within the nucleoplasm and associated with chromatin.[11] Although poly(A)$^+$ TERRAs are more stable than non-polyadenylated transcripts,[11,12] the mechanisms regulating TERRA stability remain to be defined.

The association of TERRA with telomeres is dependent on its telomeric 3′ end, which mediates the interaction with telomere-binding proteins[13–18] and the formation of RNA:DNA hybrids, or R-loops, at chromosome ends.[16,19–27]

At telomeres, TERRA mediates multiple important functions, including regulation of telomere replication,[28] heterochromatin formation,[13] recruitment of telomerase,[29–32] and homologous recombination among telomeres in cancer cells using alternative lengthening mechanisms of telomeres (ALT).[16,19,23,24,33] Altered telomeric localization and depletion of TERRA result in impaired telomere function.[1,14,15,34–36] Furthermore, deregulation of TERRA transcription by the use of modified transcription activator-like effectors (TALEs) induced telomere dysfunction.[33,37] These findings indicate that proper TERRA expression and

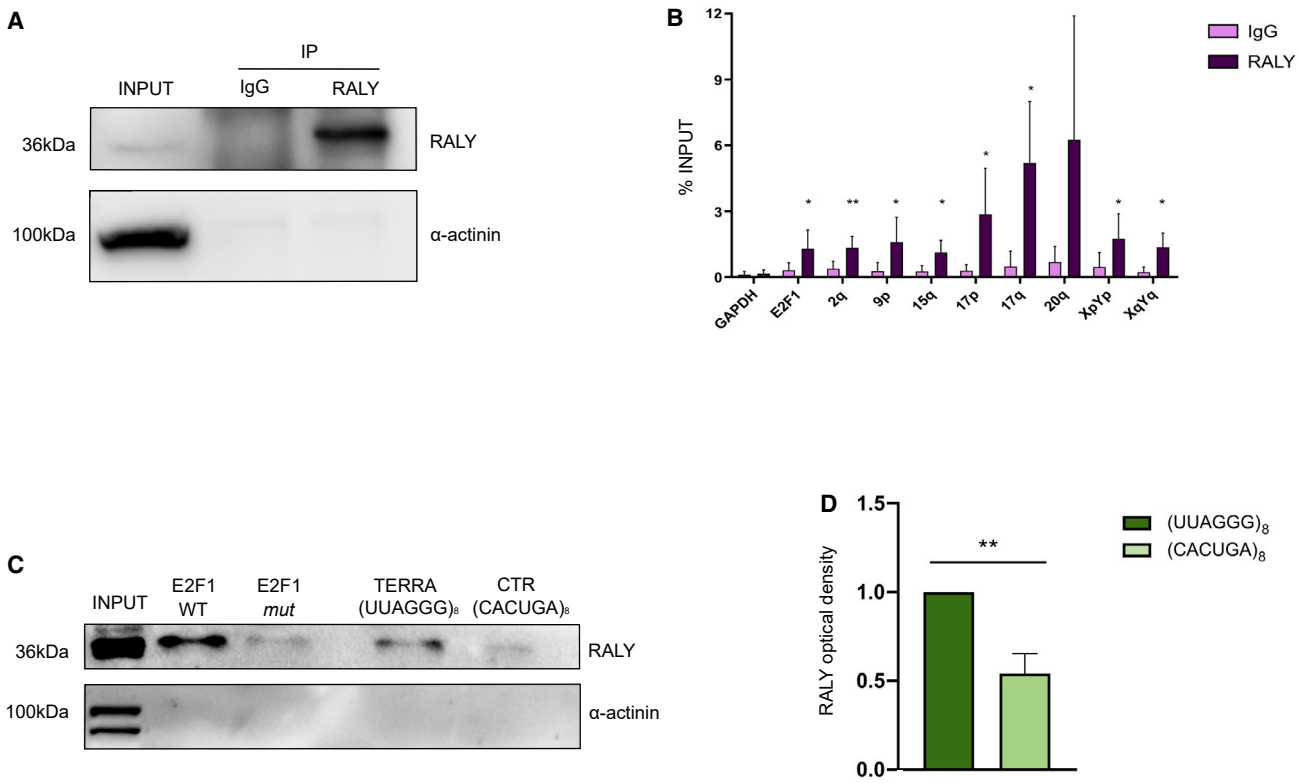

Figure 1. TERRA transcripts interact with RALY

(A) Western blot analysis for RALY and α-actinin proteins in RALY immunoprecipitates (IPs), control IPs (IgG), and input from nuclear protein lysates of HeLa cells. The experiment was repeated at least two times.

(B) TERRA is enriched in RALY IPs. qRT-PCR analyses to assess the indicated TERRA transcripts in RALY IP and IgG IP samples. *E2F1* and *GAPDH* mRNAs were used as positive and negative controls for RALY interaction, respectively. Data are shown as percentage of input and represent the mean and SEM from at least two independent experiments. Statistical analyses were performed using two-tailed unpaired t test versus *GAPDH* (negative control). *$p < 0.05$, **$p < 0.01$.

(C) Western blot analysis for RALY and α-actinin proteins upon RNA pull-down from nuclear protein lysates of HeLa cells. Two oligonucleotides were used: a biotinylated TERRA-mimicking oligonucleotide consisting of 8 repeats of the G-rich telomeric RNA sequence ($UUAGGG_8$) and a control oligonucleotide ($CACUGA_8$). RNA probes for E2F1 wild type (WT) and mutated form (*mut*) were used as positive and negative controls of RALY interaction, respectively. The experiment was repeated at least two times.

(D) Quantification of western blot RALY signal pulled down by ($UUAGGG_8$) or ($CACUGA_8$) biotinylated oligos. Data shown represent mean and SEM. n = 2. Statistical analyses were performed using two-tailed unpaired t test; **$p < 0.01$.

localization are essential to telomere function. Nevertheless, the molecular mechanisms of TERRA biogenesis remain elusive.

RALY is a member of the RNA-binding protein heterogeneous nuclear ribonucleoproteins (hnRNPs) family that preferentially binds U-rich regions within the 3′ UTR of RNAs.[38,39] RALY plays roles in several biological processes related to RNA metabolism, splicing, RNA stability, and transcription.[39–43] Recently, RALY was identified as a component of the TERRA interactome in mouse embryonic stem cells[14] and in human osteosarcoma U2OS cells,[44] suggesting a possible role in the biology of TERRA, yet the TERRA-RALY interaction remained uninvestigated.

Here, we show that RALY binds TERRA in human cancer cells, playing an active role in regulating TERRA levels in a telomere-specific manner. In the attempt to gain mechanistic insights on this process, we found that TERRA polyadenylation occurs preferentially on transcripts expressed from specific telomeres. Polyadenylation represents the main determinant for the stability of the poly(A)$^+$ TERRA transcripts, while poly(A)$^-$ TERRA molecules are stabilized by RALY. Notably, we report that TERRA transcripts interact with the poly(A)-binding protein nuclear 1 (PABPN1) and that TERRA stability is regulated by the concerted action of PABPN1 and RALY in a telomere-specific manner. Our findings provide unexpected insights into the mechanisms controlling TERRA levels in human cancer cells.

RESULTS

TERRA transcripts interact with RALY

We investigated whether TERRA transcripts interact with RALY by RNA immunoprecipitation (RIP) experiments. A RALY-specific antibody enabled us to immunoprecipitate the endogenous RALY protein from HeLa nuclear extracts (Figure 1A). qRT-PCR analyses revealed an enrichment of TERRA from all telomeres analyzed, suggesting a possible interaction between RALY and TERRA (Figure 1B). Since RALY preferentially binds the 3′

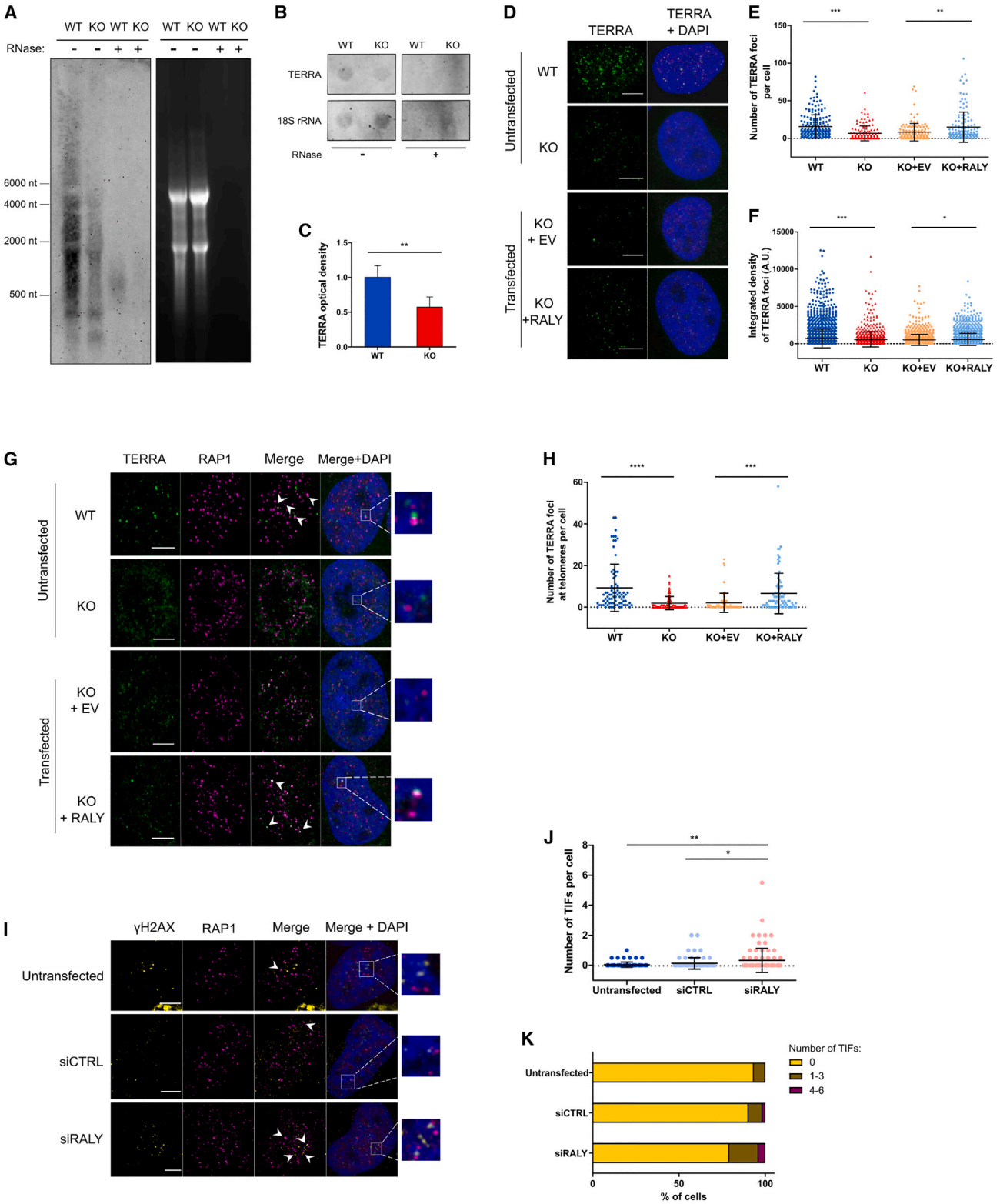

(legend on next page)

UTRs,[39] we hypothesized that it might interact with the 3′ end sequence of TERRA, which is common to all TERRA transcripts. To investigate this possibility, we assessed the interaction between RALY and a biotinylated TERRA-mimicking oligonucleotide. Incubation of HeLa nuclear extracts with the TERRA-mimicking oligonucleotide retrieved RALY (Figures 1C and 1D). In contrast, RALY was barely detected in the pull-down experiments performed using a TERRA-mutated oligonucleotide. As expected, the negative control α-actinin protein was not detected (Figure 1C). These findings indicate that TERRA interacts with RALY via its 3′ end.

TERRA levels are regulated by RALY

To investigate the role of RALY in the biology of TERRA, we analyzed TERRA levels in HeLa RALY knockout (KO) cells generated by CRISPR-Cas9.[39] Northern blot analyses revealed lower TERRA levels compared with HeLa control cells (Figure 2A). Furthermore, RNA dot blot analyses showed a marked decrease of TERRA signal in RALY KO cells compared with control cells (Figures 2B and 2C). To visualize TERRA transcripts in fixed cells, we performed single-molecule inexpensive RNA fluorescence *in situ* hybridization (smiFISH).[45,46] As expected, we observed the formation of discrete TERRA foci in the nucleus of control cells (Figures 2D and S1A). In contrast, RALY KO cells showed a significant decrease in the number of TERRA foci per cell (Figure 2E) and less intense foci (Figure 2F). Importantly, reexpression of RALY in KO cells restored the number and intensity of TERRA foci, indicating that the decrease in TERRA signal is dependent on RALY (Figures 2E, 2F, and S1B). To further validate these results, we transfected HeLa cells with RALY-targeting small interfering RNAs (siRNAs) (Figure S1C). smiFISH analyses indicated a decrease in the number of TERRA foci per cell in siRALY-transfected cells (Figure S1D). Together, these results indicate that RALY regulates TERRA levels in cells.

To study whether decreased TERRA levels would result in impaired TERRA localization, we performed smiFISH for TERRA followed by immunofluorescence (IF) for RAP1, a telomere-binding protein and Shelterin complex subunit (Figure 2G). By these experiments, we observed a marked decrease in the number of TERRA foci localizing at telomeres in RALY KO cells (Figure 2H) and siRALY-transfected cells (Figure S1E). Importantly, reexpression of RALY in KO cells restored the number of telomeric TERRA foci at telomeres, confirming that the impaired localization of TERRA is RALY dependent (Figure 2H). Since an impaired telomeric localization of TERRA and a decrease of TERRA levels associate with telomere dysfunction,[1,15,34] we investigated the presence of DNA damage at telomeres upon RALY depletion (Figure 2I). Transfection of siRALY resulted in an increased percentage of cells positive for telomere dysfunction-induced foci (TIFs) and an increased number of TIFs per cell (Figures 2J and 2K). We tested whether increased DNA damage at telomeres correlates with R-loop formation by performing RNASEH1-chromatin immunoprecipitation (R-ChIP) experiments in RALY-depleted cells or control cells.[47] To this aim, we generated clones expressing the RNaseH1 mutant D210N, which binds R-loops without leading to their degradation due to defective enzymatic activity.[47] qPCR analysis of chromatin bound to the RNaseH1 mutant D210N showed no differences in R-loop formation at subtelomeres in RALY-depleted cells and HeLa control cells (Figures S1F and S1G), suggesting that RALY does not influence R-loop formation at subtelomeres. Altogether, our findings show that RALY depletion results in a downregulation of TERRA, impaired localization of TERRA transcripts at telomeres, and increased TIF formation.

Figure 2. TERRA levels are regulated by RALY

(A) Northern blot analysis of TERRA from HeLa WT and HeLa RALY KO cells. Total RNA was resolved on agarose gel (right), and membrane hybridization was performed using a probe hybridizing with the telomeric repeat tract of TERRA (TERRA probe) (left). RNase A-treated samples were loaded as control for the specificity of the signal. The experiment was repeated two times.

(B) RNA dot blot analysis using TERRA probe or 18S rRNA. Total RNA was extracted from HeLa WT and HeLa RALY KO cells. RNase A-treated samples were analyzed as control for the specificity of the signal. The experiment was repeated four times.

(C) Quantification of the RNA dot blot TERRA signals normalized over 18S RNA signals. Data shown represent mean and SEM. n = 4.

(D) Detection of TERRA in fixed cells by smiFISH in HeLa WT, RALY KO, RALY KO transfected with empty vector (KO + EV), and RALY KO transfected with RALY-expressing vector (KO + RALY). Nuclei were stained by DAPI. The experiment was repeated two times.

(E) Quantification of the number of TERRA foci per cell detected by smiFISH. Data shown represent mean and SD. n = 2. At least 100 nuclei were analyzed for each sample.

(F) Quantification of TERRA foci integrated density in the indicated conditions. Data are shown in arbitrary units representing mean and SD. n = 2. At least 100 nuclei were analyzed for each sample.

(G) Detection of telomeric TERRA foci by smiFISH for TERRA and IFs for Rap1 in the indicated conditions. DAPI was used to stain nuclei. Insets show TERRA and RAP1 foci co-localizing (untransfected WT and transfected KO + RALY) and non-co-localizing (untransfected KO and transfected KO + EV). The experiment was repeated two times.

(H) Quantification of the number of telomeric TERRA foci per cell as detected by smiFISH/IF in the indicated conditions. Data shown represent mean and SD. n = 2. At least 130 nuclei were analyzed for each sample.

(I) IF experiment using anti-γH2AX and anti-Rap1 antibodies performed in HeLa cells untransfected or transfected with siRNA CTR (siCTRL) or with RALY-targeting siRNA (siRALY). Nuclei were stained by DAPI. Insets show γH2AX and RAP1 foci not co-localizing (untransfected and siCTR) and co-localizing (siRALY). The experiment was repeated two times.

(J) Quantification of telomere dysfunction-induced foci (TIFs) per cell as detected by Rap1 and γH2AX immunostaining in the indicated conditions. Data shown represent mean and SD. n = 2. At least 120 nuclei were analyzed for each sample.

(K) Distribution of TIFs per cell. Data represent percentage of cells showing the indicated number of TIFs in untransfected cells and cells transfected with siCTRL or siRALY. Graph related to (J). n = 2. Scale bars: 5 μm.

For statistical analyses, two-tailed unpaired t test was used in (C) and two-tailed unpaired t test with Welch's correction in (E), (F), (H), and (J); *$p < 0.05$, **$p < 0.01$, ***$p < 0.001$, ****$p < 0.0001$.

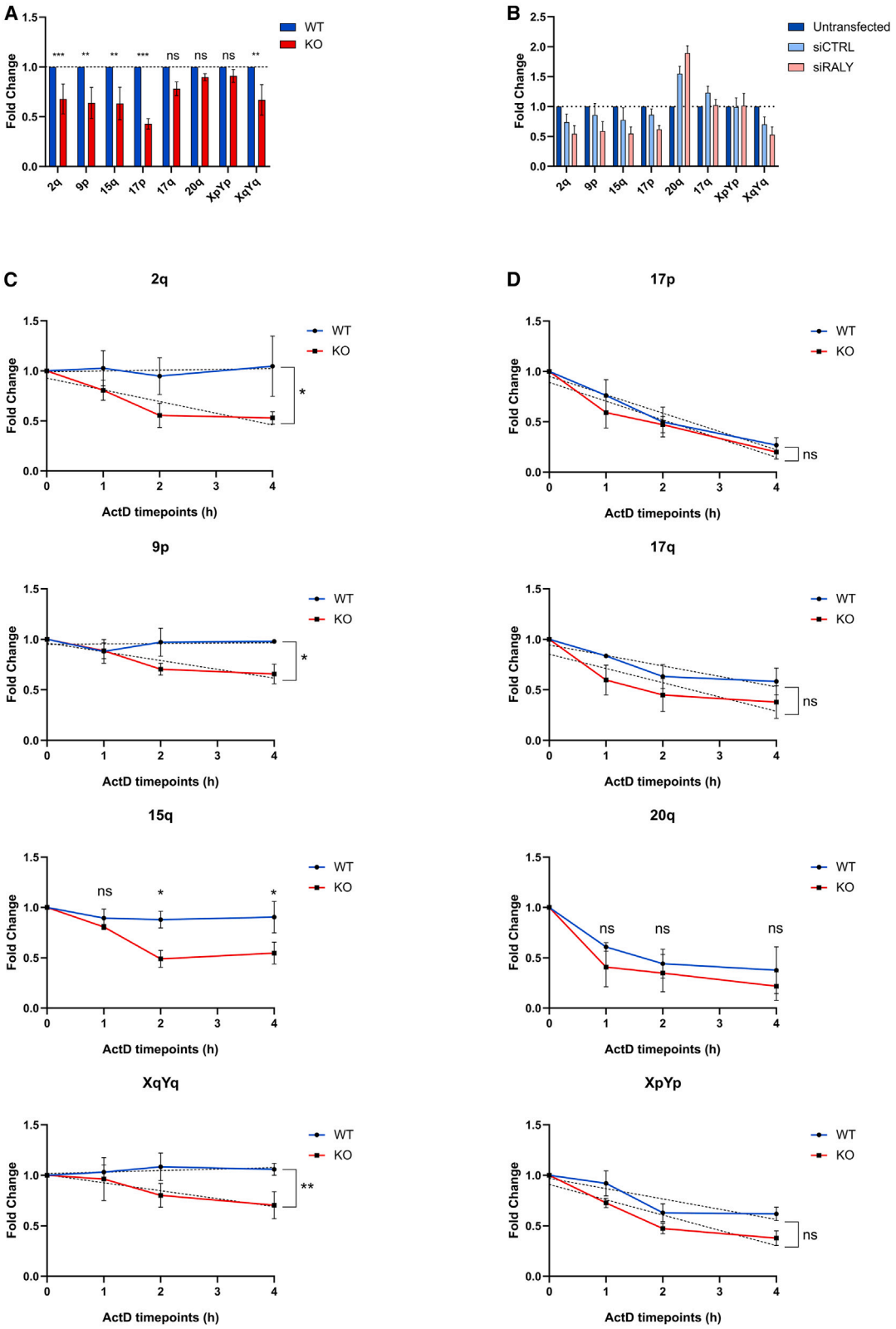

(legend on next page)

TERRA stability is regulated by RALY in a telomere-specific manner

To gain further insights into the role of RALY in the biology of TERRA, we analyzed TERRA levels from single telomeres by qRT-PCR. These analyses revealed a decrease in TERRA levels in RALY KO cells from most, although not all, telomeres analyzed (Figures 3A and S2A). Importantly, reexpression of exogenous RALY in the KO cells restored TERRA levels to wild-type (WT) conditions (Figure S2B), despite an effect of the transfection reagent on TERRA expression (Figure S2C), indicating that TERRA downregulation depends on RALY. In addition, RALY depletion resulted in decreased TERRA levels (Figure 3B). Notably, among the analyzed TERRA subpopulations, the levels of TERRA transcripts expressed from telomeres 17q, 20q, and XpYp were not affected by RALY KO (Figure 3A) or RALY depletion (Figure 3B). Together, these results indicate that TERRA levels are regulated by RALY in a telomere-specific manner.

In light of these findings, we investigated the stability of TERRA transcripts expressed from different telomeres in RALY KO cells. We treated RALY KO and WT cells with actinomycin D to block transcription and assessed TERRA levels at various time points (Figures 3C and 3D). *β-actin*, *c-myc*, and *GAPDH* mRNAs were included in the analyses for normalization and as controls (Figures S2D and S2E). Interestingly, by analyzing TERRA levels in WT cells, we observed that TERRA molecules retain different stability depending on their telomere of origin (Figures 3C and 3D). Furthermore, we found that TERRA stability is impaired in RALY KO cells in a telomere-specific manner. Indeed, TERRA transcripts expressed from telomeres 2q, 9p, 15q, and XqYq showed a significantly impaired stability (Figure 3C), while the stability of TERRA from telomeres 17p, 17q, 20q, and XpYp remained unaltered (Figure 3D). Strikingly, the levels of 17q-, 20q-, and XpYp-TERRA were also unaffected by RALY KO and RALY depletion (Figures 3A and 3B). Altogether, these findings suggest that RALY regulates TERRA levels in a telomere-specific manner by stabilizing specific subpopulations of TERRA transcripts.

TERRA transcripts are polyadenylated in a telomere-specific manner

Since TERRA stability depends on polyadenylation,[11] we investigated the extent of polyadenylation of TERRA transcripts expressed from different telomeres. To this aim, we reverse transcribed total RNA from HeLa cells with either a telomeric repeat-specific primer (TERRA RT) or an oligo-dT primer (oligo-dT RT). qPCR analyses detected telomeres 17q-, 20q-, and XpYp-TERRA from both TERRA RT and oligo-dT RT samples; conversely, telomeres 2q-, 9p-, 15q-, 17p-, and XqYq-TERRA were predominantly detected from TERRA RT cDNA (Figures 4A and S3A). These findings suggest that TERRA polyadenylation occurs preferentially at specific telomeres.

To confirm this possibility, we measured TERRA enrichment in poly(A)$^+$ and poly(A)$^-$ RNA fractions isolated from HeLa cells. *GAPDH*, *E2F1*, and *18S rRNA* were included as fractionation controls. Interestingly, TERRA expressed from telomeres 17q, 20q, and XpYp were the most enriched TERRA subpopulations in the poly(A)$^+$ fraction, while telomeres 2q-, 9p-, 15q-, 17p-, and XqYq-TERRA were predominantly detected in the poly(A)$^-$ fraction (Figures 4B and S3B). Notably, the same pattern of TERRA transcripts enrichment was detected in poly(A)$^+$ and poly(A)$^-$ fractions obtained from HCT116, MCF7, and U2OS cells (Figures 4C–4E and S3C–S3E). These findings further suggest that polyadenylation of TERRA occurs in a telomere-specific manner and that it is independent of the cell types.

RNA polyadenylation is regulated by PABPN1, which binds the RNA and stimulates poly(A) polymerase (PAP) activity.[48] To assess the interaction between PABPN1 and TERRA, we immunoprecipitated the PABPN1 protein and performed qRT-PCR analyses to detect TERRA transcripts (Figures 4F and 4G). Interestingly, most TERRA subpopulations were found enriched in the PABPN1 pull-down compared with immunoglobulin G (IgG). Telomeres 17q-, 20q-, and XpYp-TERRA were the most enriched TERRA subpopulations in the PABPN1 IP samples (Figures 4G and S3F). These findings indicate that among the TERRA transcripts analyzed, PABPN1 mainly interacts with 17q-, 20q-, and XpYp-TERRA, supporting our findings that these TERRA transcripts are preferentially polyadenylated with respect to the other TERRA subpopulations analyzed.

The mechanism of TERRA polyadenylation in human cells remains unclear. Since RALY interacts with TERRA, we verified whether it may influence TERRA polyadenylation. To this aim, we performed qPCR analyses of RNA obtained from RALY KO or control cells and reverse transcribed with TERRA RT or oligo-dT primers. These experiments revealed no differences in the TERRA polyadenylation pattern (Figure S4A), indicating that RALY expression is not required for TERRA polyadenylation. In line with these findings, ChIP experiments showed that RALY does not bind to telomeres (Figures S4B and S4C), suggesting that it exerts its function on TERRA post-transcriptionally. To investigate whether TERRA polyadenylation occurs co-transcriptionally, nuclear run-on (NRO) transcription was performed in isolated nuclei in the presence of bromouridine.[49] Labeled

Figure 3. TERRA stability is regulated by RALY in a telomere-specific manner

(A) qRT-PCR analyses of TERRA expression from the indicated telomeres performed from total RNA extracted from WT and RALY KO HeLa cells. Data are shown as fold change over HeLa WT representing mean and SEM. n = 4. Primers' amplification efficiencies were validated for all primer pairs (Table S1). Ct absolute values of TERRA levels are shown in Figure S2A.

(B) qRT-PCR analyses of TERRA expression from the indicated telomeres performed from total RNA extracted from HeLa cells untransfected and transfected with siCTRL or siRALY. Data are shown as fold change over untransfected cells (dashed line) and represent mean and SEM. n = 2.

(C and D) qRT-PCR analyses of TERRA expression from the indicated telomeres in HeLa WT and HeLa RALY KO cells at different time points after actinomycin D treatment. Data are shown as fold change over untreated cells and represent mean and SEM. n = 3.

For statistical analyses, in (A), a two-tailed unpaired t test was used; in (C) and (D), a two-tailed unpaired t test was performed between WT and KO regression lines slopes for 2q-, 9p-, 17p-, 17q-, XpYp-, and XqYq-TERRA; and for 15q- and 20q-TERRA, two-tailed unpaired t test was performed between the single WT and KO actinomycin D time points because linear regression did not fit the points; ns, not-significant, *p < 0.05, **p < 0.01, ***p < 0.001.

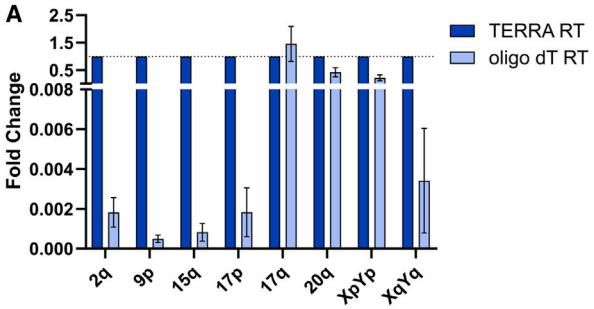

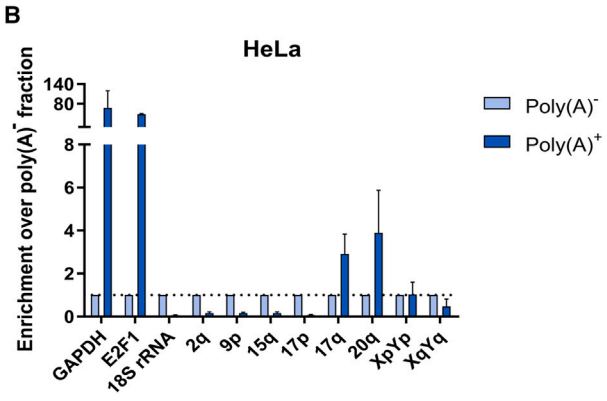

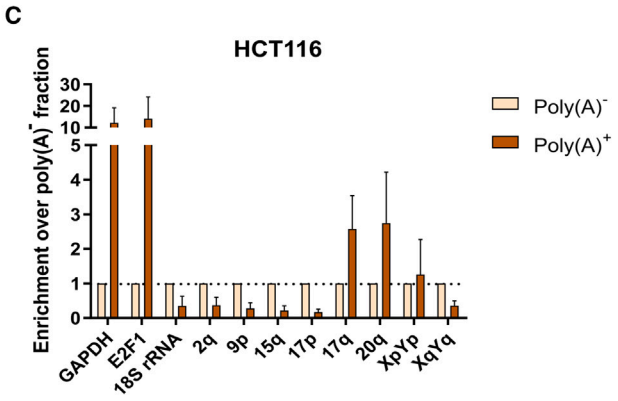

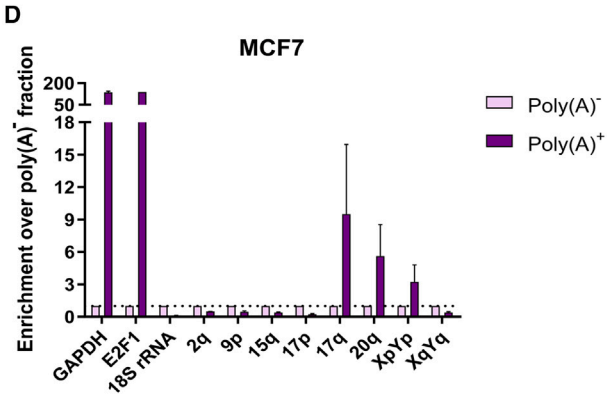

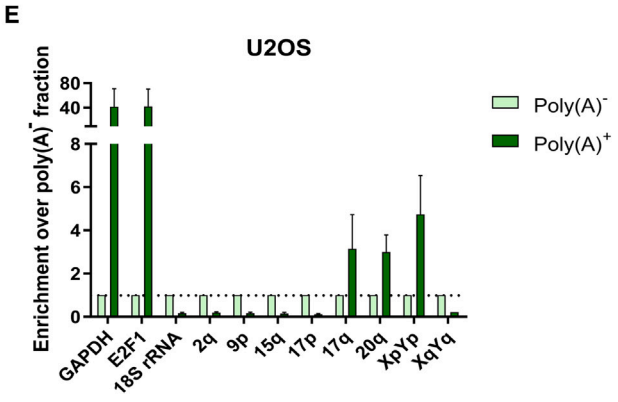

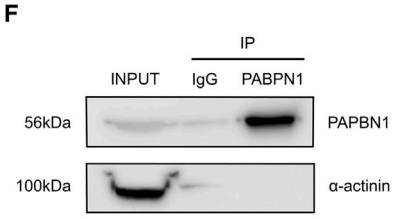

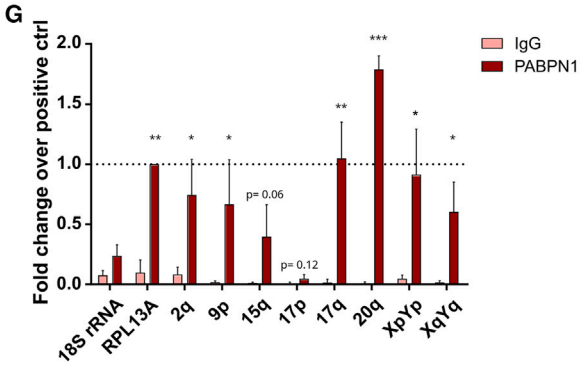

(legend on next page)

nascent transcripts were immunocaptured using an anti-BrdU antibody and analyzed by qPCR upon reverse transcription using the oligo-dT primer (Figure S4D). These experiments showed an increase in TERRA polyadenylation during transcription for two out of three TERRA subpopulations analyzed, suggesting that polyadenylation of most TERRA transcripts occurs co-transcriptionally.

R-loop formation impacts transcription termination in human cells.[50] Furthermore, recent evidence indicate that R-loop structures can regulate the RNA polyadenylation process in Arabidopsis.[51] To test whether R-loops may influence TERRA polyadenylation, we generated HeLa clones overexpressing RNase H1 or its mutant form, which is unable to degrade R-loops.[47] RNaseH1 overexpression did not influence the TERRA polyadenylation pattern, suggesting that R-loops are not involved in the TERRA polyadenylation process in HeLa cells (Figure S4E). Altogether, these results indicate that TERRA transcripts are polyadenylated in a telomere-specific manner. PABPN1 interacts mainly with the polyadenylated TERRA fractions, although an enrichment of non-polyadenylated TERRA transcripts is detected in PABPN1 IP samples. Most TERRA transcripts seem to be polyadenylated co-transcriptionally and neither RALY nor R-loops formation are involved in the process of TERRA polyadenylation.

TERRA stability is regulated by the interplay between RALY and PABPN1

PABPN1 has been shown to promote stability of mRNAs but also target RNAs for degradation by the nuclear exosome.[52] Since most TERRA subpopulations analyzed were found enriched in PABPN1 pull-downs, we decided to investigate a possible function of PABPN1 in the regulation of TERRA. To this aim, we depleted PABPN1 in HeLa cells using siRNAs (Figure S5A) and studied TERRA levels by qRT-PCR. Interestingly, these experiments showed a significant increase of TERRA signal upon PABPN1 depletion (Figure 5A). Elevated TERRA levels were detected from all TERRA subpopulations analyzed except for the TERRA 17p, the TERRA subpopulation showing the lowest enrichment in PABPN1 immunoprecipitates (Figure 4G). Notably, PABPN1 depletion did not affect the TERRA polyadenylation pattern (Figure S5B), indicating that PABPN1 is not involved in TERRA polyadenylation and that the increased TERRA levels detected in PABPN1-depleted cells are not due to changes in the extent of TERRA polyadenylation. These findings point to PABPN1 as a negative regulator of TERRA levels.

Since PABPN1 can promote RNA decay by targeting RNAs for exosome degradation,[52] we used siRNAs to downregulate the EXOSC3 subunit of the exosome (Figure S5A), an essential component of the complex,[53] and assessed the levels of TERRA transcripts by qRT-PCR. These analyses revealed a significant increase of TERRA levels upon EXOSC3 depletion in HeLa cells (Figure 5B). Notably, downregulation of EXOSC3 resulted in elevated TERRA levels from all TERRA subpopulations analyzed except for the TERRA 17p, in line with the results obtained upon PABPN1 depletion. Importantly, depletion of EXOSC3 did not affect PABPN1 protein levels, and PABPN1 downregulation did not alter EXOSC3 levels (Figure S5A). Thus, TERRA levels are regulated by both PABPN1 and EXOSC3. To gain insights into the mechanism of PABPN1-mediated TERRA regulation, we performed actinomycin D experiments to investigate the stability of TERRA transcripts upon PABPN1 depletion. Interestingly, the downregulation of PABPN1 resulted in a significant increase in the stability of three out of four non-polyadenylated TERRA subpopulations (Figure 5C). The stability of TERRA 17p remained unchanged (Figure S5C), in line with the unaltered levels detected upon PABPN1 depletion (Figure 5A). Conversely, no differences in stability were detected for the poly(A)$^+$ TERRA subpopulations studied (Figure 5D). These findings suggest a role of PABPN1 in regulating poly(A)$^-$ TERRA stability. On the other hand, PABPN1 downregulation may also influence TERRA transcription. Indeed, the poly(A)$^-$ 2q TERRA and the poly(A)$^+$ 17q, 20q, and XpYp TERRA transcripts are upregulated upon PABPN1 depletion, although no significant changes in their stability were detected.

Interestingly, depletion of PABPN1 or EXOSC3 in RALY KO cells did not result in TERRA upregulation from any subtelomere analyzed (Figures 5E, 5F, and S5D). Conversely, PABPN1-depleted RALY KO cells showed downregulation of both poly(A)$^-$ and poly(A)$^+$ TERRA transcripts compared with PABPN1-depleted HeLa cells (Figure 5G). The decreased TERRA levels correlate with impaired stability for both poly(A)$^+$ and poly(A)$^-$ TERRAs (Figure 5H). These findings point to RALY and PABPN1 as important regulators of TERRA stability in HeLa cells.

DISCUSSION

In the present study, we provide insight into the mechanisms regulating TERRA stability in human cancer cells. We show that TERRA interacts with the hnRNP RALY and that this

Figure 4. TERRA transcripts are polyadenylated in a telomere-specific manner

(A) qRT-PCR analyses of TERRA expressed from the indicated telomeres using TERRA RT or oligo-dt RT primers. Data are shown as fold change over TERRA RT samples and represent mean and SEM. n = 3.

(B–E) qRT-PCR analyses of TERRA transcripts expressed from the indicated telomeres in poly(A)$^+$ and poly(A)$^-$ fractions obtained from total RNA of HeLa (B), HCT116 (C), MCF7 (D), and U2OS cells (E). Poly(A)$^+$ transcripts (*GAPDH* and *E2F1*) and a poly(A)$^-$ RNA (*18S rRNA*) were included in the analyses. Data are shown as fold change over poly(A)$^-$ fraction and represent mean and SEM. n = 2.

(F) Western blot analysis for PABPN1 and α-actinin proteins in PABPN1 IPs, control IPs (IgG), and input from nuclear protein lysates of HeLa cells. The experiment was repeated three times.

(G) qRT-PCR analyses to assess the indicated TERRA subpopulations in PABPN1 IP and IgG IP samples. *RPL13-A* and *rRNA18S* were used as positive and negative controls for PABPN1 interaction, respectively. Data are shown as enrichment over RPL13-A and represent the mean and SEM. n = 3.

In (G), one-way ANOVA (Dunnett's multiple comparison) test was performed; *p < 0.05, **p < 0.01, ***p < 0.001. Ct absolute values of TERRA levels (A–E) and TERRA enrichment in PABPN1 RIP experiments (G) are shown in Figure S3.

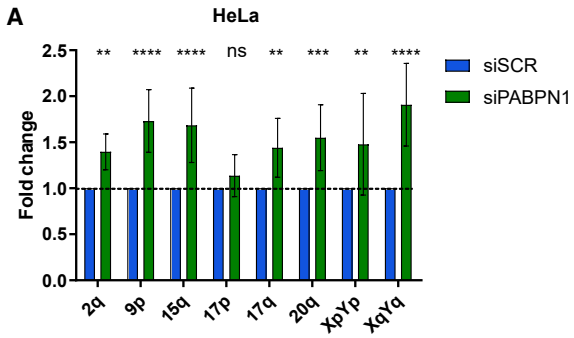

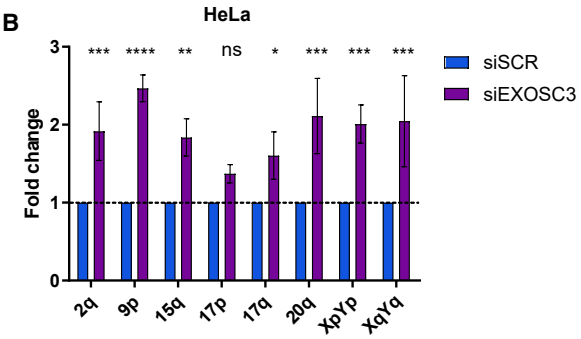

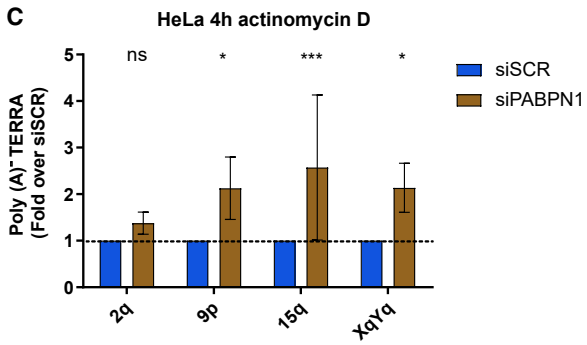

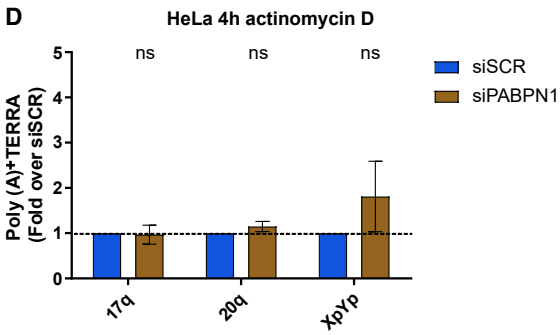

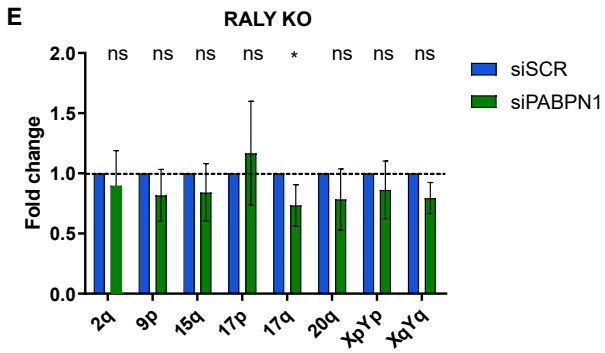

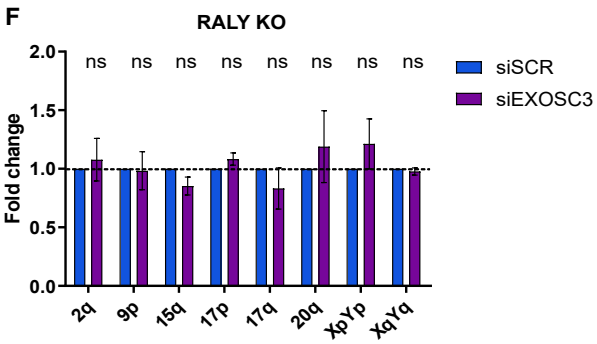

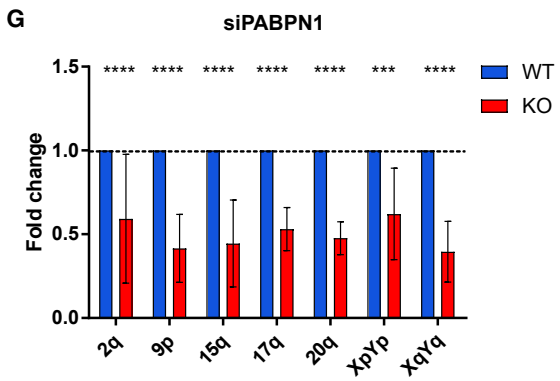

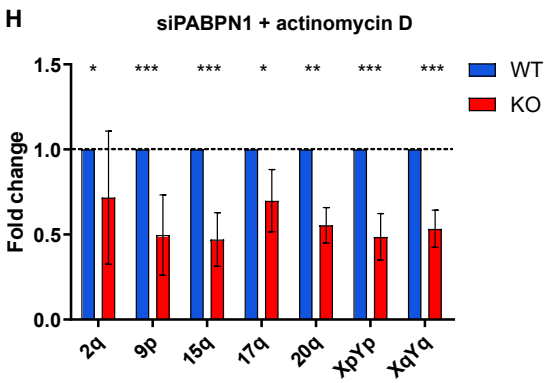

(legend on next page)

interaction stabilizes TERRA transcripts in a telomere-specific manner. Our findings indicate that the binding with RALY is a key determinant for the stability of poly(A)$^-$ TERRA molecules, which account for more than 90% of the TERRA population in HeLa cells.[10] RIP experiments revealed that both poly(A)$^-$ and poly(A)$^+$ TERRA transcripts can interact with RALY. While this interaction can be mediated by the telomeric repeat tract of TERRA (Figure 1C), we cannot exclude that the subtelomeric sequences of the transcripts contribute to the binding. This scenario might explain the differences in the enrichment of the various TERRA subpopulations in RALY immunoprecipitates.

In addition, we report that TERRA polyadenylation occurs on transcripts expressed from specific telomeres, with poly(A)$^+$ TERRA transcripts detected from telomeres 17q, 20q, and XpYp in HeLa, MCF7, and HCT116 cells, which are telomerase-positive human cancer cell lines, as well as U2OS cells, a telomerase-negative human cancer cell line that maintains telomeres via ALT mechanisms. These findings suggest that the molecular details of TERRA polyadenylation are to some extent conserved among human cell lines and independent of the telomere maintenance mechanisms.

The TERRA polyadenylation mechanism has been enigmatic ever since the discovery of polyadenylated TERRA transcripts because no canonical poly(A) sites are present within the telomeric repeat sequences. In their landmark study on TERRA polyadenylation, Porro and colleagues assessed TERRA stability by northern blot, which enabled the quantification of the total population of TERRA, showing that the poly(A)$^+$ TERRA fraction is more stable than the poly(A)$^-$.[11] Here, we use qRT-PCR analyses to study TERRA transcripts expressed from distinct telomeres and found that TERRA stability also varies depending on its telomere of origin. Furthermore, biochemical labeling of nascent RNA molecules suggests that the poly(A) tail addition to TERRA occurs co-transcriptionally, with levels of poly(A)$^+$ TERRA molecules expressed from telomeres 20q and XpYp increasing during transcription (Figure S4D). Notably, in these experiments, the levels of polyadenylated telomere 17q-TERRA remained stable, suggesting that differences in the polyadenylation mechanism might exist among telomeres. We also provide evidence that TERRA poly(A) tail addition does not depend on PABPN1 and that neither RALY nor R-loops are involved in this process.

Polyadenylation has been shown to be influenced by the transcription rate of genes and m^{6}A RNA modifications, as well as the CCR4-Not RNA decay complex; all these processes represent important elements mediating transcription-regulated poly(A) tail formation and transcript stability.[54] Intriguingly, a recent study indicates that TERRA transcripts are m^{6}A modified within subtelomeric sequences by the METTL3 enzyme. This modification contributes to TERRA stability and telomere function in ALT cancer cells.[55] It will be interesting to investigate whether the m^{6}A modification plays any role in TERRA polyadenylation and if it influences TERRA decay in telomerase-positive cells.

Importantly, we provide evidence that TERRA levels are regulated by PABPN1 and the RNA exosome. Depletion of PABPN1 or EXOSC3 resulted in increased TERRA levels from all telomeres analyzed, except telomere 17p-TERRA. These findings also suggest that 17p-TERRA transcripts are regulated differently from other TERRA molecules. In this regard, differently from the other poly(A)$^+$ TERRA populations studied, telomere 17p-TERRA levels were found reduced in RALY KO cells without changes in the stability of the transcripts (Figure 3D). Moreover, in these experiments, telomere 17p-TERRA was also detected as the most unstable among the TERRA molecules analyzed, with its levels approximating to zero after 4 h of actinomycin D treatment, suggesting that it may undergo different stabilization and/or decay processes.

PABPN1 RIP experiments indicate that both poly(A)$^-$ and poly(A)$^+$ TERRA transcripts can interact with PABPN1 (Figure 4G). While PABPN1 is well known to bind the poly(A) tail of transcripts,[56] the mechanism of its interaction with poly(A)$^-$ TERRA molecules needs to be elucidated. PABPN1 can promote RNA decay as part of the poly(A) tail exosome-targeting connection (PAXT), which directs RNA species for nuclear exosome degradation.[52] The ZFC3H1 subunit of this complex interacts with components of the Cap-binding complex (CBC).[52] The PAXT-CBC interaction may represent a mechanism of PABPN1 recruitment to non-polyadenylated TERRA molecules, as most TERRA transcripts contain a 7mG cap.[11] In accordance with the role of PABPN1 in the decay process of poly(A)$^-$ TERRA transcripts, depletion of PABPN1 resulted in increased stability of most poly(A)$^-$ TERRA subpopulations interacting with PABPN1. Notably, inhibition of the nuclear exosome resulted in a more than 2-fold increase in TERRA expression levels from multiple telomeres (Figure 5B). This increase in expression exceeds the upregulation of TERRA detected upon PABPN1 depletion (Figure 5A), suggesting that multiple pathways may target

Figure 5. TERRA stability is regulated by the interplay between RALY and PABPN1

(A) qRT-PCR analyses of TERRA expressed from the indicated telomeres in HeLa cells after 72 h transfection of PABPN1-targeting siRNA (siPABPN1) or the control scrambled siRNA (siSCR). Data are shown as fold change over siSCR and represent mean and SD. n = 5.

(B) qRT-PCR analyses of TERRA expression in HeLa cells after 72 h transfection of EXOSC3-targeting siRNA (siEXOSC3) or the control siSCR. Data are shown as fold change over siSCR and represent mean and SD. n = 2.

(C and D) qRT-PCR analyses of TERRA levels from the indicated telomeres in siSCR and siPABPN1 HeLa cells after 4 h of actinomycin D treatment. Data were normalized over DMSO-treated samples and are shown as fold change over siSCR cells. Data shown represent mean and SD. n = 3.

(E and F) qRT-PCR analyses of TERRA levels in HeLa RALY KO cells after 72 h transfection of siPABPN1 (E), siEXOSC3 (F), and siSCR (E and F). Data are shown as fold change over siSCR and represent mean and SD. n = 5 (E) and n = 2 (F).

(G) qRT-PCR analyses of TERRA expressed from the indicated telomeres in HeLa WT and RALY KO cells after 72 h transfection of siPABPN1 or siSCR. Data were normalized over siSCR control samples and are shown as fold change over HeLa WT. Data shown represent mean and SD. n = 6.

(H) qRT-PCR analyses of TERRA levels in siPABPN1-transfected HeLa WT and RALY KO cells upon 4 h of actinomycin D treatment. Data were normalized over DMSO-treated samples and are shown as fold change over HeLa WT. Data shown represent mean and SD from at least two biological replicates. In these experiments, two-tailed unpaired t test was used for statistical analyses; ns, not-significant, *p < 0.05, **p < 0.01, ***p < 0.001.

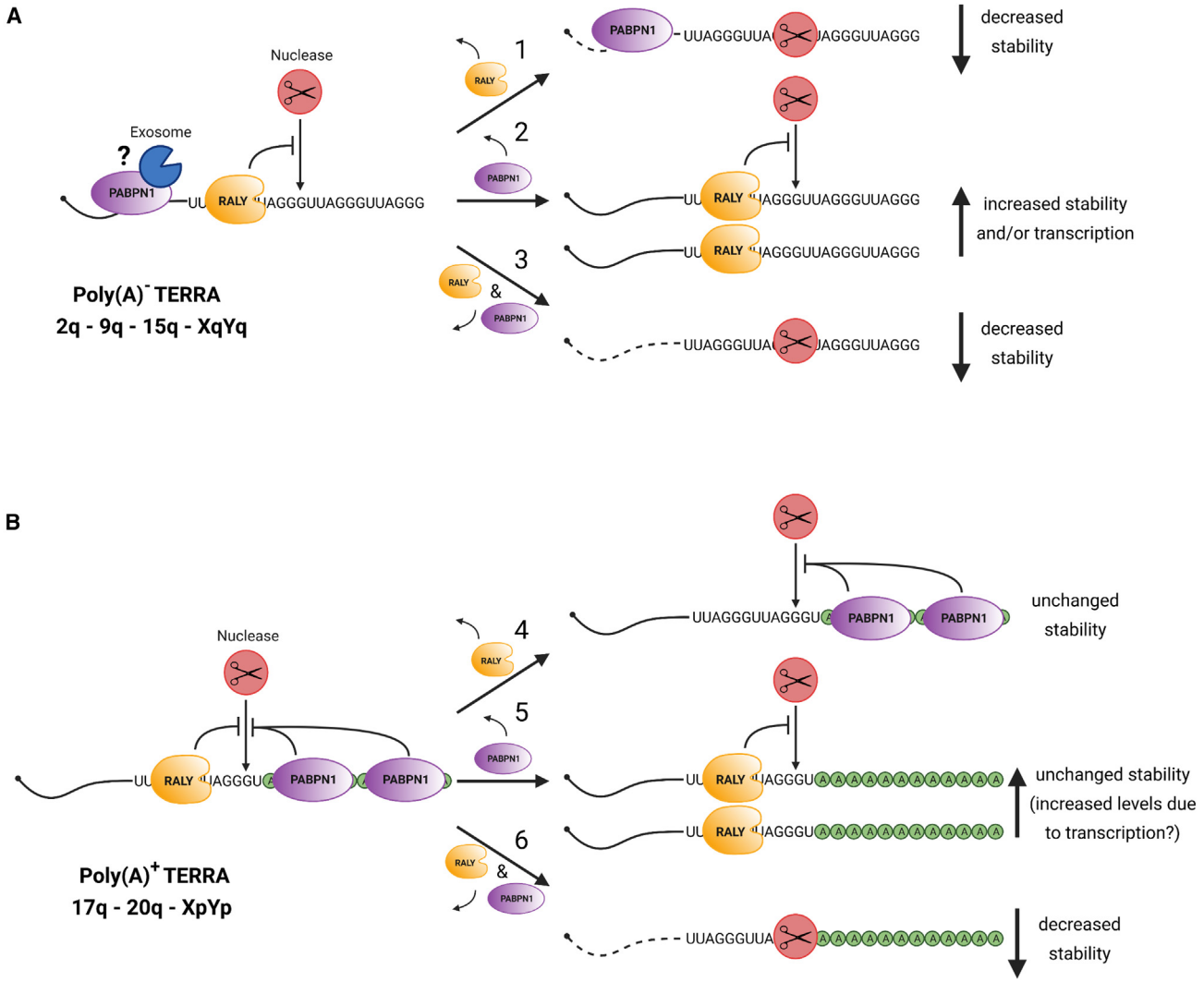

Figure 6. Proposed model: TERRA transcripts are polyadenylated in a telomere-specific manner, and their levels and stability are regulated by the concerted action of RALY and PABPN1 through mechanisms influenced by the poly(A) tail

(A) Poly(A)$^-$ TERRA transcripts interact with RALY and PABPN1. RALY binds the telomeric 3′ end sequence of TERRA molecules protecting them from degradation. PABPN1 promotes poly(A)$^-$ TERRA decay possibly by targeting them for exosome degradation. (1) The absence of RALY results in TERRA degradation and consequent decrease of TERRA stability; (2) removal of PABPN1 leads to augmented TERRA levels due to increased stability (9p-, 15q-, and XpYp-TERRA) and possibly transcription (2q-TERRA); (3) the absence of both RALY and PABPN1 results in decreased TERRA levels due to TERRA degradation.

(B) Poly(A)$^+$ TERRA transcripts are bound by RALY and PABPN1. The presence of the poly(A) tail enables further recruitment of PABPN1 compared with poly(A)$^-$ TERRA. In these conditions, both RALY and PABPN1 act redundantly in protecting TERRA molecules from degradation. (4) In the absence of RALY, poly(A)$^+$ TERRA transcript stability is unchanged, as PABPN1 protects them from degradation; similarly, (5) poly(A)$^+$ TERRA stability is not influenced by the removal of PABPN1 since, under this condition, RALY prevents their degradation. Long-term PABPN1 depletion may influence the transcription of poly(A)$^+$ TERRA molecules, leading to their increased levels. (6) The absence of both RALY and PABPN1 results in poly(A)$^+$ TERRA degradation and consequent decreased stability compared with RALY-expressing cells. This image was created using BioRender.

TERRA for degradation by the exosome. A potential candidate is the nuclear exosome-targeting (NEXT) complex, which targets non-polyadenylated RNAs for exosome degradation.[57]

Of note, PABPN1 depletion resulted in no changes in poly(A)$^+$ TERRA transcript stability, despite their increased levels. These findings suggest that TERRA transcription from a subset of telomeres may also be influenced by downregulation of PABPN1. However, at this stage, we cannot rule out that this effect can be indirect. In future studies, the use of a recently developed approach to rapidly downregulate proteins involved in RNA decay pathways may help shed light on this process.[58] Surprisingly, in RALY KO cells, depletion of PABPN1 or EXOSC3 did not result in elevated TERRA levels, suggesting that RALY contributes to the TERRA regulation by PABPN1 and the exosome.

Furthermore, the absence of both PABPN1 and RALY resulted in decreased levels and impaired the stability of both poly(A)$^-$ and poly(A)$^+$ TERRAs compared with PABPN1-depleted cells.

Based on these results, we propose a model in which poly(A)$^-$ and poly(A)$^+$ TERRA transcripts are bound by RALY and PABPN1, acting as regulators of TERRA levels in human cancer cells (Figure 6). Poly(A)$^-$ TERRA molecules are stabilized by RALY. Conversely, PABPN1 promotes TERRA decay possibly by targeting poly(A)$^-$ TERRA transcripts for exosome degradation (Figure 6A). Importantly, the increased stability of poly(A)$^-$ TERRA upon PABPN1 depletion depends on RALY, underlining an interplay between RALY and PABPN1 in the regulation of TERRA levels. We hypothesize that poly(A)$^-$ TERRA transcripts are degraded by multiple RNA decay pathways. RALY inhibits a TERRA decay process not involving PABPN1. Thus, the downregulation of PABPN1 results in the stabilization of poly(A)$^-$ TERRA transcripts in a RALY-dependent manner. If RALY is absent, poly(A)$^-$ TERRA degradation can take place, with or without PABPN1. The presence of different RNA decay pathways targeting specific RNAs has been previously described. For example, the human telomerase RNA hTR is processed by the poly(A)-specific ribonuclease PARN, and it is targeted for degradation by the nuclear exosome through the activity of the trf4p/5p-Air1p/2p-Mtr4p polyadenylation (TRAMP) and NEXT complexes.[59] Competition between these decay pathways enables the maintenance of the proper hTR levels in cells and contributes to hTR maturation.[59–61]

Notably, the role of RALY and PABPN1 in the regulation of poly(A)$^+$ TERRA transcripts is different from their function in the control of poly(A)$^-$ TERRA molecules. Indeed, the absence of RALY or PABPN1 does not affect the stability of poly(A)$^+$ TERRA transcripts. Conversely, depletion of PABPN1 in RALY KO cells results in impaired stability of both poly(A)$^-$ and poly(A)$^+$ TERRA molecules compared with PABPN1-depleted cells expressing RALY. We hypothesize that RALY and PABPN1 act redundantly in protecting poly(A)$^+$ TERRA molecules from degradation (Figure 6B). The presence of the poly(A) tail may thus represent a key determinant for the function of RALY and PABPN1 in TERRA regulation. The molecular mechanisms controlling poly(A)$^+$ TERRA stability will require further investigation. It will be important to study whether oligoadenylated transcripts are present within the TERRA population. Such modified TERRA molecules could be generated by the activity of the TRF4 or TRF5 oligo(A)-polymerases within the TRAMP complex directing RNAs for exosome degradation.[62–64]

In summary, our findings unveil an unexpected role of the hnRNP RALY and PABPN1 in the control of TERRA stability, which may set the stage for future investigations aimed at elucidating the polyadenylation mechanisms and decay pathways targeting TERRA transcripts in human cancer cells. Given the importance of TERRA transcripts in telomere function, any insight into the mechanisms regulating TERRA levels may lead to breakthroughs in the telomere field. Our results also indicate that TERRA polyadenylation occurs in a telomere-specific manner. Given the different biological features of poly(A)$^-$ versus poly(A)$^+$ TERRA, it can be hypothesized that different telomeres may trigger distinct TERRA-mediated responses.

Limitations of the study

In this work, we did not provide information on the length of the poly(A) tail of TERRA transcripts. Despite several attempts, technical issues prevented us from sequencing the 3′ end of the polyadenylated TERRA molecules. As a consequence, we cannot exclude that a fraction of the polyadenylated TERRA transcripts include oligoadenylated transcripts since the oligo-dT reverse transcription and the RNA fractionation protocols used in this study may, in principle, enable the detection of such molecules if their oligo(A) tails are sufficiently long. It remains to be defined which RNA decay mechanism targeting TERRA is inhibited by RALY. Furthermore, additional studies are required to reveal the mechanism of telomere-specific TERRA polyadenylation in human cells.

STAR★METHODS

Detailed methods are provided in the online version of this paper and include the following:

- KEY RESOURCES TABLE
- RESOURCE AVAILABILITY
  - Lead contact
  - Materials availablity
  - Data and code availability
- EXPERIMENTAL MODEL AND SUBJECT DETAILS
  - Cell culture and transfections
- METHOD DETAILS
  - Western blot
  - RNA immunoprecipitation
  - RNA pull-down
  - Northern blot
  - RNA dot-blot
  - Quantitative real-time PCR (qRT-PCR)
  - Primer efficiency test
  - Single molecule inexpensive fluorescent *in situ* hybridization (SmiFISH)
  - SmiFISH/immunofluorescence (SmiFISH/IF)
  - Immunofluorescence (IF)
  - Isolation of poly(A)$^+$ and poly(A)$^-$ RNA fractions
  - Nuclear run-on (NRO)
  - Chromatin immunoprecipitation (ChIP)
  - RNaseH1-chromatin immunoprecipitation (R-ChIP)
  - DNA dot-blot
- QUANTIFICATION AND STATISTICAL ANALYSES

SUPPLEMENTAL INFORMATION

Supplemental information can be found online at https://doi.org/10.1016/j.celrep.2023.112406.

ACKNOWLEDGMENTS

We are thankful to Michela Rocuzzo for assistance with microscopy image analyses and to Pascal Chartrand and Emmanuelle Querido for assistance with the smiFISH protocol. We are grateful to Dr. Anabelle Decottignies for sharing unpublished data and to Dr. Alessio Zippo and Dr. Massimo Pizzato for sharing reagents. We are thankful to Dr. Marie-Laure Baudet for the critical comments on the manuscript. We thank the Advanced Imaging Facility at CIBIO for the assistance with the imaging procedures. The research leading to these results

has received funding from the Italian Association for Cancer Research (AIRC) under MFAG 2019, project ID 22840 - P.I. Cusanelli Emilio. This work was also supported by the AIL Trento - Associazione Italiana contro le Leucemie, Linfomi e Mieloma to Paolo Macchi. T.T. was supported by AIRC under MFAG 2020 (project ID 24883).

AUTHOR CONTRIBUTIONS

Conceptualization, V.S., J.R., A.G., P.M., and E.C.; methodology, V.S., J.R., A.G., T.T., A.R., R.M., I.G., P.M., and E.C.; investigation, V.S., J.R., A.G., A.R., R.M., T.T., and L.Z.; writing – original draft, E.C.; writing – review & editing, V.S., J.R., A.G., T.T., A.R., P.M., and E.C.; funding acquisition, P.M. and E.C.; resources, I.G., P.M., and E.C.; supervision, P.M. and E.C.

DECLARATION OF INTERESTS

The authors declare no competing interests.

INCLUSION AND DIVERSITY

We support inclusive, diverse, and equitable conduct of research.

Received: October 14, 2021
Revised: January 25, 2023
Accepted: March 31, 2023

REFERENCES

1. Azzalin, C.M., Reichenbach, P., Khoriauli, L., Giulotto, E., and Lingner, J. (2007). Telomeric repeat containing RNA and RNA surveillance factors at mammalian chromosome ends. Science *318*, 798–801. https://doi.org/10.1126/science.1147182.
2. Bah, A., Wischnewski, H., Shchepachev, V., and Azzalin, C.M. (2012). The telomeric transcriptome of Schizosaccharomyces pombe. Nucleic Acids Res. *40*, 2995–3005. https://doi.org/10.1093/nar/gkr1153.
3. Greenwood, J., and Cooper, J.P. (2012). Non-coding telomeric and subtelomeric transcripts are differentially regulated by telomeric and heterochromatin assembly factors in fission yeast. Nucleic Acids Res. *40*, 2956–2963. https://doi.org/10.1093/nar/gkr1155.
4. Luke, B., Panza, A., Redon, S., Iglesias, N., Li, Z., and Lingner, J. (2008). The Rat1p 5' to 3' exonuclease degrades telomeric repeat-containing RNA and promotes telomere elongation in Saccharomyces cerevisiae. Mol. Cell *32*, 465–477. https://doi.org/10.1016/j.molcel.2008.10.019.
5. Schoeftner, S., and Blasco, M.A. (2008). Developmentally regulated transcription of mammalian telomeres by DNA-dependent RNA polymerase II. Nat. Cell Biol. *10*, 228–236. https://doi.org/10.1038/ncb1685.
6. Diman, A., and Decottignies, A. (2018). Genomic origin and nuclear localization of TERRA telomeric repeat-containing RNA: from Darkness to Dawn. FEBS J. *285*, 1389–1398. https://doi.org/10.1111/febs.14363.
7. Azzalin, C.M., and Lingner, J. (2015). Telomere functions grounding on TERRA firma. Trends Cell Biol. *25*, 29–36. https://doi.org/10.1016/j.tcb.2014.08.007.
8. Nergadze, S.G., Farnung, B.O., Wischnewski, H., Khoriauli, L., Vitelli, V., Chawla, R., Giulotto, E., and Azzalin, C.M. (2009). CpG-island promoters drive transcription of human telomeres. RNA *15*, 2186–2194. https://doi.org/10.1261/rna.1748309.
9. Porro, A., Feuerhahn, S., Delafontaine, J., Riethman, H., Rougemont, J., and Lingner, J. (2014). Functional characterization of the TERRA transcriptome at damaged telomeres. Nat. Commun. *5*, 5379. https://doi.org/10.1038/ncomms6379.
10. Azzalin, C.M., and Lingner, J. (2008). Telomeres: the silence is broken. Cell Cycle *7*, 1161–1165. https://doi.org/10.4161/cc.7.9.5836.
11. Porro, A., Feuerhahn, S., Reichenbach, P., and Lingner, J. (2010). Molecular dissection of telomeric repeat-containing RNA biogenesis unveils the presence of distinct and multiple regulatory pathways. Mol. Cell Biol. *30*, 4808–4817. https://doi.org/10.1128/MCB.00460-10.
12. Feuerhahn, S., Iglesias, N., Panza, A., Porro, A., and Lingner, J. (2010). TERRA biogenesis, turnover and implications for function. FEBS Lett. *584*, 3812–3818. https://doi.org/10.1016/j.febslet.2010.07.032.
13. Arnoult, N., Van Beneden, A., and Decottignies, A. (2012). Telomere length regulates TERRA levels through increased trimethylation of telomeric H3K9 and HP1alpha. Nat. Struct. Mol. Biol. *19*, 948–956. https://doi.org/10.1038/nsmb.2364.
14. Chu, H.P., Cifuentes-Rojas, C., Kesner, B., Aeby, E., Lee, H.G., Wei, C., Oh, H.J., Boukhali, M., Haas, W., and Lee, J.T. (2017). TERRA RNA antagonizes ATRX and protects telomeres. Cell *170*, 86–101.e16. https://doi.org/10.1016/j.cell.2017.06.017.
15. Deng, Z., Norseen, J., Wiedmer, A., Riethman, H., and Lieberman, P.M. (2009). TERRA RNA binding to TRF2 facilitates heterochromatin formation and ORC recruitment at telomeres. Mol. Cell *35*, 403–413. https://doi.org/10.1016/j.molcel.2009.06.025.
16. Petti, E., Buemi, V., Zappone, A., Schillaci, O., Broccia, P.V., Dinami, R., Matteoni, S., Benetti, R., and Schoeftner, S. (2019). SFPQ and NONO suppress RNA:DNA-hybrid-related telomere instability. Nat. Commun. *10*, 1001. https://doi.org/10.1038/s41467-019-08863-1.
17. Scheibe, M., Arnoult, N., Kappei, D., Buchholz, F., Decottignies, A., Butter, F., and Mann, M. (2013). Quantitative interaction screen of telomeric repeat-containing RNA reveals novel TERRA regulators. Genome Res. *23*, 2149–2157. https://doi.org/10.1101/gr.151878.112.
18. Viceconte, N., Loriot, A., Lona Abreu, P., Scheibe, M., Fradera Sola, A., Butter, F., De Smet, C., Azzalin, C.M., Arnoult, N., and Decottignies, A. (2021). PAR-TERRA is the main contributor to telomeric repeat-containing RNA transcripts in normal and cancer mouse cells. RNA *27*, 106–121. https://doi.org/10.1261/rna.076281.120.
19. Arora, R., Lee, Y., Wischnewski, H., Brun, C.M., Schwarz, T., and Azzalin, C.M. (2014). RNaseH1 regulates TERRA-telomeric DNA hybrids and telomere maintenance in ALT tumour cells. Nat. Commun. *5*, 5220. https://doi.org/10.1038/ncomms6220.
20. Balk, B., Maicher, A., Dees, M., Klermund, J., Luke-Glaser, S., Bender, K., and Luke, B. (2013). Telomeric RNA-DNA hybrids affect telomere-length dynamics and senescence. Nat. Struct. Mol. Biol. *20*, 1199–1205. https://doi.org/10.1038/nsmb.2662.
21. Graf, M., Bonetti, D., Lockhart, A., Serhal, K., Kellner, V., Maicher, A., Jolivet, P., Teixeira, M.T., and Luke, B. (2017). Telomere length determines TERRA and R-loop regulation through the cell cycle. Cell *170*, 72–85.e14. https://doi.org/10.1016/j.cell.2017.06.006.
22. Hu, Y., Bennett, H.W., Liu, N., Moravec, M., Williams, J.F., Azzalin, C.M., and King, M.C. (2019). RNA-DNA hybrids support recombination-based telomere maintenance in fission yeast. Genetics *213*, 431–447. https://doi.org/10.1534/genetics.119.302606.
23. Lee, Y.W., Arora, R., Wischnewski, H., and Azzalin, C.M. (2018). TRF1 participates in chromosome end protection by averting TRF2-dependent telomeric R loops. Nat. Struct. Mol. Biol. *25*, 147–153. https://doi.org/10.1038/s41594-017-0021-5.
24. Silva, B., Pentz, R., Figueira, A.M., Arora, R., Lee, Y.W., Hodson, C., Wischnewski, H., Deans, A.J., and Azzalin, C.M. (2019). FANCM limits ALT activity by restricting telomeric replication stress induced by deregulated BLM and R-loops. Nat. Commun. *10*, 2253. https://doi.org/10.1038/s41467-019-10179-z.
25. Feretzaki, M., Pospisilova, M., Valador Fernandes, R., Lunardi, T., Krejci, L., and Lingner, J. (2020). RAD51-dependent recruitment of TERRA lncRNA to telomeres through R-loops. Nature *587*, 303–308. https://doi.org/10.1038/s41586-020-2815-6.
26. Vohhodina, J., Goehring, L.J., Liu, B., Kong, Q., Botchkarev, V.V., Jr., Huynh, M., Liu, Z., Abderazzaq, F.O., Clark, A.P., Ficarro, S.B., et al. (2021). BRCA1 binds TERRA RNA and suppresses R-Loop-based

telomeric DNA damage. Nat. Commun. *12*, 3542. https://doi.org/10.1038/s41467-021-23716-6.

27. Ghisays, F., Garzia, A., Wang, H., Canasto-Chibuque, C., Hohl, M., Savage, S.A., Tuschl, T., and Petrini, J.H.J. (2021). RTEL1 influences the abundance and localization of TERRA RNA. Nat. Commun. *12*, 3016. https://doi.org/10.1038/s41467-021-23299-2.
28. Beishline, K., Vladimirova, O., Tutton, S., Wang, Z., Deng, Z., and Lieberman, P.M. (2017). CTCF driven TERRA transcription facilitates completion of telomere DNA replication. Nat. Commun. *8*, 2114. https://doi.org/10.1038/s41467-017-02212-w.
29. Cusanelli, E., Romero, C.A.P., and Chartrand, P. (2013). Telomeric noncoding RNA TERRA is induced by telomere shortening to nucleate telomerase molecules at short telomeres. Mol. Cell *51*, 780–791. https://doi.org/10.1016/j.molcel.2013.08.029.
30. Farnung, B.O., Brun, C.M., Arora, R., Lorenzi, L.E., and Azzalin, C.M. (2012). Telomerase efficiently elongates highly transcribing telomeres in human cancer cells. PLoS One *7*, e35714. https://doi.org/10.1371/journal.pone.0035714.
31. Lalonde, M., and Chartrand, P. (2020). TERRA, a multifaceted regulator of telomerase activity at telomeres. J. Mol. Biol. *432*, 4232–4243. https://doi.org/10.1016/j.jmb.2020.02.004.
32. Moravec, M., Wischnewski, H., Bah, A., Hu, Y., Liu, N., Lafranchi, L., King, M.C., and Azzalin, C.M. (2016). TERRA promotes telomerase-mediated telomere elongation in Schizosaccharomyces pombe. EMBO Rep. *17*, 999–1012. https://doi.org/10.15252/embr.201541708.
33. Silva, B., Arora, R., Bione, S., and Azzalin, C.M. (2021). TERRA transcription destabilizes telomere integrity to initiate break-induced replication in human ALT cells. Nat. Commun. *12*, 3760. https://doi.org/10.1038/s41467-021-24097-6.
34. Avogaro, L., Querido, E., Dalachi, M., Jantsch, M.F., Chartrand, P., and Cusanelli, E. (2018). Live-cell imaging reveals the dynamics and function of single-telomere TERRA molecules in cancer cells. RNA Biol. *15*, 787–796. https://doi.org/10.1080/15476286.2018.1456300.
35. López de Silanes, I., Graña, O., De Bonis, M.L., Dominguez, O., Pisano, D.G., and Blasco, M.A. (2014). Identification of TERRA locus unveils a telomere protection role through association to nearly all chromosomes. Nat. Commun. *5*, 4723. https://doi.org/10.1038/ncomms5723.
36. López de Silanes, I., Stagno d'Alcontres, M., and Blasco, M.A. (2010). TERRA transcripts are bound by a complex array of RNA-binding proteins. Nat. Commun. *1*, 33. https://doi.org/10.1038/ncomms1032.
37. Silva, B., Arora, R., and Azzalin, C.M. (2022). The alternative lengthening of telomeres mechanism jeopardizes telomere integrity if not properly restricted. Proc. Natl. Acad. Sci. USA *119*, e2208669119. https://doi.org/10.1073/pnas.2208669119.
38. Michaud, E.J., Bultman, S.J., Stubbs, L.J., and Woychik, R.P. (1993). The embryonic lethality of homozygous lethal yellow mice (Ay/Ay) is associated with the disruption of a novel RNA-binding protein. Genes Dev. *7*, 1203–1213. https://doi.org/10.1101/gad.7.7a.1203.
39. Rossi, A., Moro, A., Tebaldi, T., Cornella, N., Gasperini, L., Lunelli, L., Quattrone, A., Viero, G., and Macchi, P. (2017). Identification and dynamic changes of RNAs isolated from RALY-containing ribonucleoprotein complexes. Nucleic Acids Res. *45*, 6775–6792. https://doi.org/10.1093/nar/gkx235.
40. Bondy-Chorney, E., Baldwin, R.M., Didillon, A., Chabot, B., Jasmin, B.J., and Côté, J. (2017). RNA binding protein RALY promotes Protein Arginine Methyltransferase 1 alternatively spliced isoform v2 relative expression and metastatic potential in breast cancer cells. Int. J. Biochem. Cell Biol. *91*, 124–135. https://doi.org/10.1016/j.biocel.2017.07.008.
41. Cornella, N., Tebaldi, T., Gasperini, L., Singh, J., Padgett, R.A., Rossi, A., and Macchi, P. (2017). The hnRNP RALY regulates transcription and cell proliferation by modulating the expression of specific factors including the proliferation marker E2F1. J. Biol. Chem. *292*, 19674–19692. https://doi.org/10.1074/jbc.M117.795591.
42. Gasperini, L., Rossi, A., Cornella, N., Peroni, D., Zuccotti, P., Potrich, V., Quattrone, A., and Macchi, P. (2018). The hnRNP RALY regulates PRMT1 expression and interacts with the ALS-linked protein FUS: implication for reciprocal cellular localization. Mol. Biol. Cell *29*, 3067–3081. https://doi.org/10.1091/mbc.E18-02-0108.
43. Sallam, T., Jones, M.C., Gilliland, T., Zhang, L., Wu, X., Eskin, A., Sandhu, J., Casero, D., Vallim, T.Q.d.A., Hong, C., et al. (2016). Feedback modulation of cholesterol metabolism by the lipid-responsive non-coding RNA LeXis. Nature *534*, 124–128. https://doi.org/10.1038/nature17674.
44. Guh, C.Y., Shen, H.J., Chen, L.W., Chiu, P.C., Liao, I.H., Lo, C.C., Chen, Y., Hsieh, Y.H., Chang, T.C., Yen, C.P., et al. (2022). XPF activates break-induced telomere synthesis. Nat. Commun. *13*, 5781. https://doi.org/10.1038/s41467-022-33428-0.
45. Querido, E., Sfeir, A., and Chartrand, P. (2020). Imaging of telomerase RNA by single-molecule inexpensive FISH combined with immunofluorescence. STAR Protoc. *1*, 100104. https://doi.org/10.1016/j.xpro.2020.100104.
46. Tsanov, N., Samacoits, A., Chouaib, R., Traboulsi, A.M., Gostan, T., Weber, C., Zimmer, C., Zibara, K., Walter, T., Peter, M., et al. (2016). smiFISH and FISH-quant - a flexible single RNA detection approach with super-resolution capability. Nucleic Acids Res. *44*, e165. https://doi.org/10.1093/nar/gkw784.
47. Chen, L., Chen, J.Y., Zhang, X., Gu, Y., Xiao, R., Shao, C., Tang, P., Qian, H., Luo, D., Li, H., et al. (2017). R-ChIP using inactive RNase H reveals dynamic coupling of R-loops with transcriptional pausing at gene promoters. Mol. Cell *68*, 745–757.e5. https://doi.org/10.1016/j.molcel.2017.10.008.
48. Kerwitz, Y., Kühn, U., Lilie, H., Knoth, A., Scheuermann, T., Friedrich, H., Schwarz, E., and Wahle, E. (2003). Stimulation of poly(A) polymerase through a direct interaction with the nuclear poly(A) binding protein allosterically regulated by RNA. EMBO J. *22*, 3705–3714. https://doi.org/10.1093/emboj/cdg347.
49. Roberts, T.C., Hart, J.R., Kaikkonen, M.U., Weinberg, M.S., Vogt, P.K., and Morris, K.V. (2015). Quantification of nascent transcription by bromouridine immunocapture nuclear run-on RT-qPCR. Nat. Protoc. *10*, 1198–1211. https://doi.org/10.1038/nprot.2015.076.
50. Ginno, P.A., Lim, Y.W., Lott, P.L., Korf, I., and Chédin, F. (2013). GC skew at the 5' and 3' ends of human genes links R-loop formation to epigenetic regulation and transcription termination. Genome Res. *23*, 1590–1600. https://doi.org/10.1101/gr.158436.113.
51. Xu, C., Wu, Z., Duan, H.C., Fang, X., Jia, G., and Dean, C. (2021). R-loop resolution promotes co-transcriptional chromatin silencing. Nat. Commun. *12*, 1790. https://doi.org/10.1038/s41467-021-22083-6.
52. Meola, N., Domanski, M., Karadoulama, E., Chen, Y., Gentil, C., Pultz, D., Vitting-Seerup, K., Lykke-Andersen, S., Andersen, J.S., Sandelin, A., and Jensen, T.H. (2016). Identification of a nuclear exosome decay pathway for processed transcripts. Mol. Cell *64*, 520–533. https://doi.org/10.1016/j.molcel.2016.09.025.
53. Belair, C., Sim, S., Kim, K.Y., Tanaka, Y., Park, I.H., and and; and Wolin, S.L. (2019). The RNA exosome nuclease complex regulates human embryonic stem cell differentiation. J. Cell Biol. *218*, 2564–2582. https://doi.org/10.1083/jcb.201811148.
54. Slobodin, B., Bahat, A., Sehrawat, U., Becker-Herman, S., Zuckerman, B., Weiss, A.N., Han, R., Elkon, R., Agami, R., Ulitsky, I., et al. (2020). Transcription dynamics regulate poly(A) tails and expression of the RNA degradation machinery to balance mRNA levels. Mol. Cell *78*, 434–444.e5. https://doi.org/10.1016/j.molcel.2020.03.022.
55. Chen, L., Zhang, C., Ma, W., Huang, J., Zhao, Y., and Liu, H. (2022). METTL3-mediated m6A modification stabilizes TERRA and maintains telomere stability. Nucleic Acids Res. *50*, 11619–11634. https://doi.org/10.1093/nar/gkac1027.
56. Nemeth, A., Krause, S., Blank, D., Jenny, A., Jenö, P., Lustig, A., and Wahle, E. (1995). Isolation of genomic and cDNA clones encoding bovine poly(A) binding protein II. Nucleic Acids Res. *23*, 4034–4041. https://doi.org/10.1093/nar/23.20.4034.

57. Wu, G., Schmid, M., Rib, L., Polak, P., Meola, N., Sandelin, A., and Jensen, T.H. (2020). A two-layered targeting mechanism underlies nuclear RNA sorting by the human exosome. Cell Rep. *30*, 2387–2401.e5. https://doi.org/10.1016/j.celrep.2020.01.068.

58. Gockert, M., Schmid, M., Jakobsen, L., Jens, M., Andersen, J.S., and Jensen, T.H. (2022). Rapid factor depletion highlights intricacies of nucleoplasmic RNA degradation. Nucleic Acids Res. *50*, 1583–1600. https://doi.org/10.1093/nar/gkac001.

59. Tseng, C.K., Wang, H.F., Burns, A.M., Schroeder, M.R., Gaspari, M., and Baumann, P. (2015). Human telomerase RNA processing and quality control. Cell Rep. *13*, 2232–2243. https://doi.org/10.1016/j.celrep.2015.10.075.

60. Tseng, C.K., Wang, H.F., Schroeder, M.R., and Baumann, P. (2018). The H/ACA complex disrupts triplex in hTR precursor to permit processing by RRP6 and PARN. Nat. Commun. *9*, 5430. https://doi.org/10.1038/s41467-018-07822-6.

61. Nguyen, D., Grenier St-Sauveur, V., Bergeron, D., Dupuis-Sandoval, F., Scott, M.S., and Bachand, F. (2015). A polyadenylation-dependent 3' end maturation pathway is required for the synthesis of the human telomerase RNA. Cell Rep. *13*, 2244–2257. https://doi.org/10.1016/j.celrep.2015.11.003.

62. LaCava, J., Houseley, J., Saveanu, C., Petfalski, E., Thompson, E., Jacquier, A., and Tollervey, D. (2005). RNA degradation by the exosome is promoted by a nuclear polyadenylation complex. Cell *121*, 713–724. https://doi.org/10.1016/j.cell.2005.04.029.

63. Vanácová, S., Wolf, J., Martin, G., Blank, D., Dettwiler, S., Friedlein, A., Langen, H., Keith, G., and Keller, W. (2005). A new yeast poly(A) polymerase complex involved in RNA quality control. PLoS Biol. *3*, e189. https://doi.org/10.1371/journal.pbio.0030189.

64. Wyers, F., Rougemaille, M., Badis, G., Rousselle, J.C., Dufour, M.E., Boulay, J., Régnault, B., Devaux, F., Namane, A., Séraphin, B., et al. (2005). Cryptic pol II transcripts are degraded by a nuclear quality control pathway involving a new poly(A) polymerase. Cell *121*, 725–737. https://doi.org/10.1016/j.cell.2005.04.030.

STAR★METHODS

KEY RESOURCES TABLE

REAGENT or RESOURCE	SOURCE	IDENTIFIER
Antibodies		
Rabbit polyclonal anti-RALY	Bethyl	Cat#A302-069A; RRID: AB_1604210
Rabbit polyclonal anti-PABPN1	Bethyl	Cat# A303-524A; RRID: AB_10949200
Rabbit polyclonal anti-EXOSC3	Proteintech	Cat#15062-1-AP; RRID: AB_2278183
Mouse monoclonal anti-β-Tubulin	Santa Cruz	Cat# sc-5274; RRID: AB_2288090
Mouse monoclonal anti-α-Actinin	Santa Cruz	Cat#sc-17829; RRID: AB_626633
Rabbit polyclonal anti-mouse IgG H&L (HRP)	Abcam	Cat#ab6728; RRID: AB_955440
Goat polyclonal anti-rabbit IgG H&L (HRP)	Abcam	Cat#ab6721; RRID: AB_955447
Normal rabbit polyclonal IgG	Millipore	Cat# PP64; RRID: AB_97852
Sheep anti-Digoxigenin-AP, Fab fragments	Roche	Cat#11093274910; RRID: AB_514497
Rabbit polyclonal anti-RAP1	Novus Biologicals	Cat#NB100-292; RRID: AB_10000825
Mouse monoclonal anti-phospho-Histone H2A.X	Millipore	Cat#05–636; RRID: AB_309864
Goat polyclonal anti-rabbit IgG-AF647	Thermo Fisher Scientific	Cat#A-21245; RRID: AB_2535813
Goat polyclonal anti-rabbit IgG-AF555	Thermo Fisher Scientific	Cat#A-21428; RRID: AB_2535849
Goat polyclonal anti-mouse IgG-AF488	Thermo Fisher Scientific	Cat#A-11001; RRID: AB_2534069
Mouse monoclonal anti-BrdU	Santa Cruz	Cat#sc-32323; RRID: AB_626766
Rabbit monoclonal anti-V5	Cell Signaling	Cat# 13202; RRID: AB_2687461
Chemicals, peptides, and recombinant proteins		
Oligofectamine Transfection Reagent	Invitrogen	12252011
jetPRIME Transfection Reagent	Polyplus	114–15
Actinomycin D	Gibco	11805017
Pierce Protease Inhibitor Mini Tablets	Thermo Scientific	A32955
RiboLock RNase Inhibitor	Thermo Scientific	EO0381
RNaseOUT Recombinant Ribonuclease Inhibitor	Invitrogen	10777019
Ribonucleoside Vanadyl Complex	NEB	S1402S
Dynabeads Protein G	Invitrogen	10003D
Dynabeads M-280 Streptavidin	Invitrogen	11205D
SuperSignal West Pico PLUS ECL Substrate	Thermo Scientific	34577
CDP-Star ECLSubstrate	Roche	11685627001
TRIzol Reagent	Invitrogen	15596018
Phenol/Chloroform/Isoamyl alcohol (25:24:1)	Fisher BioReagents	BP1752I400
Formaldehyde	Fisher BioReagents	BP531-500
MOPS	Fisher BioReagents	BP308-100
Formamide	AppliChem	A2156,0500
Blocking Reagent	Roche	11096176001
KAPA SYBR FAST qPCR Mastermix	KAPA Biosystems	KK4601
qPCRBIO SyGreen Mix Separate-ROX	PCR Biosystems	PB20.14–20
DNase I	Thermo Scientific	89836
RNase A	Macherey Nagel	740505
RNase T1	Thermo Scientific	EN0541
Proteinase K	Thermo Scientific	EO0491
Glycogen	Invitrogen	10814010
SuperScript III Reverse Transcriptase	Invitrogen	18080044
dNTP Set	Invitrogen	10297018
NEBuffer 3	NEB	B7003S

(*Continued on next page*)

Continued

REAGENT or RESOURCE	SOURCE	IDENTIFIER
ProLong Diamond Antifade Mountant	Invitrogen	P36965
BrUTP	Santa Cruz	sc-495784
Critical commercial assays		
DIG Oligonucleotide 3-End Labeling Kit	Roche	3353575910
Poly(A) RNA Selection Kit	Lexogen	157.96
Experimental models: Cell lines		
Human: HeLa	ATCC	CCL-2™
Human: HeLa RALY KO	Macchi Lab	Rossi et al. 2017[39]
Human: U2OS	ATCC	HTB-96™
Human: MCF7	ATCC	HTB-22™
Human: HCT116	ATCC	CCL-247™
Oligonucleotides		
siRNA, see Table S2	N/A	N/A
RT primers, see Table S2	N/A	N/A
qPCR primers, see Table S2	N/A	N/A
Blot probes, see Table S2	N/A	N/A
smiFISH probes, see Table S2	N/A	N/A
RNA pull-down oligonucleotides, see Table S2	N/A	N/A
Recombinant DNA		
pCMV6-entry	Macchi Lab	Origene #PS100001
pCMV6-entry-RALY	Macchi Lab	Gasperini et al. 2018[42]
ppyCAG_RNaseH1_WT	Zippo Lab	Addgene #111906
ppyCAG_RNaseH1_D210N	Zippo Lab	Addgene #111904
ppyCAG_RNaseH1_WKKD	Zippo Lab	Addgene #111905
Software and algorithms		
Image Lab 6.0.1	Bio-Rad	https://www.bio-rad.com/it-it/product/image-lab-software?ID=KRE6P5E8Z
ImageJ	NIH	https://imagej.net/
Prism 8.0.0	GraphPad	www.graphpad.com
BioRender	BioRender	BioRender.com

RESOURCE AVAILABILITY

Lead contact

Further information and requests for resources and reagents should be directed to and will be fulfilled by the lead contact: Emilio Cusanelli, emilio.cusanelli@unitn.it.

Materials availablity

This study did not generate new unique reagents.

Data and code availability

- All data reported in this paper will be share by the lead contact upon request.
- This paper does not report original codes.
- Any additional information required to reanalyze the data reported in this paper is available from the lead contact upon request.

EXPERIMENTAL MODEL AND SUBJECT DETAILS

Cell culture and transfections

Human cervical adenocarcinoma HeLa cells were obtained from ATCC. HeLa RALY KO cells were generated using the CRIPSR/Cas9 system to introduce a deletion spanning from exon 1 to exon 2, as described previously.[39] U2OS cells (human osteosarcoma), MCF7

(human breast adenocarcinoma) and HCT116 (human colon adenocacinoma) were obtained from ATCC. All cells were cultured in DMEM, supplemented with 10% fetal bovine serum and 1% penicillin/streptomycin at 37°C with 5% CO2. Cells were regularly tested for mycoplasma contamination. For the actinomycin D experiments, HeLa cells were treated with either 5μg/mL actinomycin D (Gibco, in DMSO) or 0.1% DMSO only as control.[41] RNA extraction was performed after 1, 2 and 4 h from the beginning of the treatment. For gene knock down experiments, cells were grown at 50–70% confluence on 10 cm Petri dishes and transfected with gene-targeting siRNAs (RALY, PABPN1, or EXOSC3) or control siRNA (SMARTpool, Dharmacon) using Oligofectamine transfection reagent (Invitrogen), according to the manufacturer's protocol. The effects of RALY, PABPN1 or EXOSC3 depletion were assessed 72 h after transfection.[39] Information on the siRNAs used in this study are present in Table S2. For the rescue experiments of RALY expression, HeLa RALY KO cells were transfected at 60–80% confluence either with PCMV6-entry empty vector or with pCMV6-entry-RALY plasmid (Origene) using jetPRIME (Polyplus) transfection reagent according to the manufacturer's protocol. Cells were then either fixed or lysed 24 h after transfection. For R-ChIP and TERRA polyadenylation analyses in RNaseH1 expressing cells, HeLa and U2OS clones expressing V5-tagged WT or mutated RNase H1 were generated by the transfection (jetPRIME - Polyplus) of ppyCAG_RNaseH1_WT, ppyCAG_RNaseH1_D210N or ppyCAG_RNaseH1_WKKD (Addgene) and selection by 60 μg/mL of Hygromycin for 2 weeks.

METHOD DETAILS

Western blot

Cells were washed with 1X PBS and lysed in lysis buffer (0.1% Triton X-100, 150 mM KCl, 50 mM HEPES, pH 7.4 and 1 mM DTT plus proteinase inhibitors mixture (Thermo Scientific), including 1 mM phenylmethylsulfonyl fluoride (PMSF)). Equal amounts of proteins were separated on 12% SDS-PAGE and blotted onto a nitrocellulose membrane (Schleicher & Schuell). Western blots were probed with the following primary antibodies: rabbit polyclonal anti-RALY (1:2000; Bethyl); rabbit polyclonal anti-PABPN1 (1:2000; Bethyl); rabbit polyclonal anti-EXOSC3 (1:2000; Proteintech); mouse monoclonal anti-β-tubulin (1:2000, Santa Cruz Biotechnology); mouse monoclonal anti-α-actinin (1:2000; Santa Cruz Biotechnology). Horseradish peroxidase (HRP)-conjugated goat anti-mouse and anti-rabbit antibodies (1:3000; Abcam) were used as secondary antibodies. The intensity of the signals was quantified by using the Volume Tools in Image Lab 6.0.1 software (Bio-Rad).

RNA immunoprecipitation

RNA immunoprecipitation was performed as previously described.[39] Briefly, HeLa cells cultured on 10 cm Petri dishes to 70%–90% of confluence were crosslinked once with 150 mJ/cm^2 at 254 nm using an UVLink UV-crosslinker (Uvitec Cambridge), then lysed for 2 h at −80°C in RIP lysis buffer (10 mM HEPES pH 7.4, 5 mM $MgCl_2$, 100 mM KCl, 2 mM EDTA pH 8, 0.5% IGEPAL, 1 mM DTT plus RNase inhibitor, including 2 mM VRC and proteinase inhibitor (Thermo Scientific)). Samples were then centrifuged at 13000 rpm for 20 min at 4°C. The supernatant was precleared for 2 h at 4°C with protein G magnetic beads (Invitrogen) and then 3 mg of lysate were incubated overnight at 4°C with either rabbit polyclonal anti-RALY antibody (3 μg; Bethyl), rabbit polyclonal anti-PABPN1 antibody (3 μg; Bethyl) or normal rabbit IgG polyclonal antibody (3 μg; Millipore). 40 μL of protein G magnetic beads were added to lysates and incubated for 2 h at 4°C. The beads were then washed five times with 1 mL of NT2 buffer (50 mM Tris–HCl pH 7.5, 150 mM NaCl, 1 mM $MgCl_2$, 2 mM EDTA pH 8, 0.05% IGEPAL, 1 mM DTT plus RNase inhibitor, including 2 mM VRC and proteinase inhibitor (Thermo Scientific)). Proteins were run on 10% SDS-PAGE for Western blot analysis. RNA was isolated with TRIzol Reagent (Invitrogen) according to manufacturer instructions using 0.5 mL of reagent per immunoprecipitated sample and input samples. RNA was then processed for qRT-PCR analysis as described below. The relative enrichment of transcripts was calculated according to the percentage of input.

RNA pull-down

Biotinylated RNA probes were purchased from Eurofins Genomics (Table S2). The TERRA-mimicking or control probes (80 pmol) were incubated with 35 μL of streptavidin-coupled Dynabeads (Invitrogen) for 20 min at room temperature in RNA Capture Buffer [20 mM Tris (pH 7.5), 1 M NaCl, 1 mM EDTA].[39,41] HeLa cells were washed with PBS and then lysed with a lysis buffer [10 mM HEPES pH 7.4, 100 mM KCl, 5 mM $MgCl_2$, 0.5% NP40, 1mM DTT plus RNase and proteinase inhibitors]. The lysate (400 μg) was incubated with biotinylated RNA probes coupled to streptavidin Dynabeads for 2 h at 4°C under rotation. Dynabeads were then washed three times with washing solution [20 mM Tris (pH 7.5), 10 mM NaCl, 0.1% Tween 20], solubilized in Laemmli reducing buffer and boiled for Western blot analysis.

Northern blot

Total RNA was extracted using TRIzol Reagent (Invitrogen) according to manufacturer instructions. 10μg of RNA was denatured for 5 min at 65°C in 1X RNA Loading Dye (Thermo Fisher Scientific) and loaded on a denaturing MOPS gel (1.2% agarose Sigma-Aldrich, 1X MOPS Fisher BioReagents, 2% formaldehyde Fisher BioReagents, in H_2O) containing 1:20000 Atlas ClearSight (Bio-atlas) dye. For RNase-A controls, 10μg of RNA was incubated with RNase A (1:200; Macherey Nagel) for 1h at 37°C before the denaturation step. The gel run was allowed for 3 h at 125 V, and the RNA was transferred overnight at room temperature (RT) through capillarity on an Amersham Hybond H^+ membrane (GE Healthcare), previously equilibrated in H_2O and 20X SSC. The

following day, the membrane was crosslinked with UV for 3 min at 1500 μJ/cm^2 on the UVP CL-1000L Longwave Crosslinker (Fisher Scientific), pre-hybridized in hybridization buffer (5X SSC, 0.1% Sarkosyl, 0.04% SDS) for 1 h at 45°C in the UVP HB-1000 Hybridizer oven (Fisher Scientific) and hybridized overnight in hybridization buffer containing 5 nM TERRA 3′-DIG probe, labeled using DIG Oligonucleotide 3′-End Labeling Kit (Roche), according to manufacturer's protocol. The membrane was washed 2 times in 2X SSC/0.1% SDS for 5 min at RT, 2 times in 0.2X SSC/0.1% SDS for 5 min at RT, 2 times in pre-heated 0.2X SSC/0.1% SDS at 37°C for 15 min and briefly in 2X SSC at RT. Then, the membrane was incubated for 1 h at RT in blocking solution (Maleic acid buffer pH 7.5 (0.1M maleic acid, 0.15M sodium chloride) containing 1% blocking reagent (Roche)) and then in blocking solution containing Anti-DIG antibody 1:10000 (Roche) for 30 min at RT. Finally, the membrane was washed 2 times for 15 min in wash buffer (Maleic buffer pH 7.5 containing 0.3% Tween 20), equilibrated in AP buffer (0.1M Tris pH 9.5, 0.1M NaCl) for 2 min at RT and prepared for detection at the ChemiDoc XRS+ (Bio-Rad) with CDP-Star Chemiluminescence Substrate (Roche), according to the manufacturer's protocol.

RNA dot-blot

4 μg of total RNA were purified from HeLa cells using TRIzol Reagent (Invitrogen), was treated with DNase I and its integrity checked by MOPS gel. Half of DNase-treated RNA was incubated with RNase A (1:200; Macherey Nagel) for 1 h at 37°C to be used as a negative control. Samples were diluted in EDTA pH 8 to a final concentration of 1 mM and the same volume of formamide (AppliChem) was added. Samples were denatured at 65°C for 10 min before blotting on an Amersham Hybond H+ membrane (GE Healthcare) using the BioDot apparatus (Bio-Rad), to obtain spots of 2 μg. After blotting, the membrane was dried under chemical hood and crosslinked with UV for 3 min per side at 120 mJ/cm^2 on the UVP CL-1000L Longwave Crosslinker (Fisher Scientific), pre-hybridized for 1 h in the UVP HB-1000 Hybridizer oven (Fisher Scientific) with pre-heated (pre)hybridization buffer (5X SSC, 0.1% sarkosyl, 0.04% SDS in H_2O) and hybridized with 5 nM 3′ DIG-labeled probes. Probe labeling was performed using DIG Oligonucleotide 3′ End-Labeling Kit (Roche) according to the manufacturer's protocol. The hybridization step was performed by incubating the membrane in (pre)hybridization buffer overnight at 50°, for TERRA detection, or 42°C, for *rRNA 18S* or *β-actin* detection. The membrane was washed 2 times for 5 min in 2X SSC/0.1% SDS at room temperature, then 2 times for 5 min in 0.5X SSC/0.1% SDS, 2 times for 15 min in pre-heated 0.5X SSC/0.1% SDS at 42°C and briefly in 2X SSC at RT. The membrane was incubated for 1 h at room temperature in blocking solution (1% Blocking Reagent, Roche, 1X Maleic Acid Buffer pH 7.5 in H_2O) and for 30 min at room temperature with an anti-DIG antibody (1:10000; Roche) in blocking solution. Finally, the membrane was washed 2 times for 30 min in wash buffer (0.3% Tween 20, 0.5X Maleic Acid Buffer pH 7.5 in H_2O), equilibrated for 2 min in AP buffer (100mM Tris-HCl pH 9.5, 100mM NaCl in H_2O) and prepared for detection at the ChemiDoc XRS+ (Bio-Rad) with CDP-Star Chemiluminescence Substrate (Roche), according to the manufacturer's protocol. The intensity of the signal was quantified by using the Volume Tools in Image Lab 6.0.1 software (Bio-Rad).

Quantitative real-time PCR (qRT-PCR)

All primers used in this study, including RT and qPCR primers, were purchased from Metabion and Eurofins Genomics and are listed in Table S2.

Total RNA was purified from cells using TRIzol Reagent (Invitrogen) according to manufacturer instructions. Briefly, cells cultured in 10cm Petri dishes were washed with 1X PBS, lysed with 1mL of TRIzol Reagent (Invitrogen), scraped and collected in Eppendorf tubes. After 15 min of incubation at RT, 200μL of chloroform were added, the tubes were vortexed and incubated 15 min at room temperature, to be centrifuged for 10 min at 4°C, 15000 rpm. 500μL of 100% isopropanol were added to the supernatant, samples were vortexed, incubated 10 min at room temperature and centrifuged for 10 min at 4°C, 15000 rpm. Pellets were washed twice with 500μL of 70% v/v ethanol by centrifugations of 10 min at 4°C, 15000 rpm before resuspension in the appropriate volume of nuclease-free H_2O. RNA concentration was assessed with the NanoDrop 1000 spectrophotometer (ThermoFisher Scientific). 3 μg of RNA were treated with DNaseI (Thermo Scientific) for 1 h at 37°C. The integrity of the RNA was assessed by a run on a MOPS gel (1% agarose, Sigma-Aldrich, 1X MOPS Fisher BioReagents in H_2O). 300 ng of DNaseI-treated RNA were reverse transcribed with either TERRA RT, oligo-(dT) RT or random hexamers primers, using the Superscript III RT enzyme (Invitrogen). 2μL of RT reaction were used for the qPCR experiments which were performed in triplicates using KAPA SYBR FAST qPCR Mastermix (KAPA Biosystems) or qPCRBIO SyGreen Mix (PCR Biosystems) in a CFX96 Thermo Cycler (Bio-Rad). The results were analyzed with Bio-Rad CFX Manager, version 2.1. The relative expression was calculated according to the $2^{-\Delta\Delta Ct}$ method normalized on *β-actin* or *GAPDH* mRNAs.

Primer efficiency test

TERRA primer pairs used for RT-qPCR were taken from the literature (see Table S2) and re-tested for amplification efficiency. Results from these analyses are shown in Table S1. In these experiments, each primer pair was tested on both HeLa genomic DNA (gDNA) and cDNA reverse-transcribed with TERRA RT primers. Ten-fold serial dilutions of gDNA or cDNA were prepared in order to have five different gDNA/cDNA concentrations and qPCR was performed for TERRA primer pairs to be tested. After qPCR, the reaction mixes were loaded and run on a 2% agarose gel to check the amplicon size. Only primer pairs amplifying the correct size amplicon were

considered for efficiency calculation, the other ones were discarded. The regression line passing through the points defined by the qPCR threshold cycles (y axes) and the -log(gDNA/cDNA dilution) (x axes) was created and primer efficiency was calculated as follows:

$$E(\%) = \left(10^{(-1/m)-1}\right) * 100$$

where m is the slope of the regression line.

Single molecule inexpensive fluorescent *in situ* hybridization (SmiFISH)

SmiFISH experiments were performed on cells grown on glass coverslips in 6-well plates. Briefly, cells were fixed in 4% PFA for 20 min at room temperature, then washed twice with 1X PBS for 2 min at room temperature and then permeabilized with 0.5% Triton X-100 (in 1X PBS) for 5 min at room temperature. Control samples were treated with 200U/mL RNase A (Macherey-Nagel) and 300U/mL RNase T1 (Thermo Scientific) for 2h at 37°C. After 2 washes in 1X PBS for 2 min at room temperature, all coverslips were incubated with Formamide Buffer (1X SSC, 15% Formamide) for 25 min at room temperature and placed upside-down in an air-tight hybridization chamber over 50μL of Hybridization buffer. The FLAP-annealed probe (40pmol TERRA probe, from Metabion, annealed with 50pmol FLAP-Cy3, from Eurofins Genomics, in 1X NEB3 buffer, New England BioLabs) was incubated in the thermocycler at 85°C for 3 min, 65°C for 3 min, 25°C for 5 min and chilled on ice. Probe sequences are listed in Table S2. Hybridization was performed overnight at 37°C. The following day, coverslips were washed once with Formamide Buffer for 2 min at RT and twice with preheated Formamide Buffer for 25 min at 37°C. After two rinses in 1X PBS, coverslips were incubated with 1μg/mL DAPI in 1X PBS for 7 min at room temperature, washed twice in 1X PBS and mounted on glass slides with ProLong Diamond Antifade mountant (Invitrogen). Coverslips were sealed the day after with nail polish. Microscopy analysis was performed using the Leica TCS SP8 confocal scanning laser microscope equipped with an Andor iXon Ultra 888 EMCCD sensor monochromatic camera. Images were acquired using a 63X/1.40 Oil objective and Leica Application Suite X (LAS X) imaging software and assembled with ImageJ.

SmiFISH/immunofluorescence (SmiFISH/IF)

SmiFISH/IF experiments were performed following the smiFISH protocol described above, with the addition of the steps for immunofluorescence described below. After washing with Formamide Buffer, cells were washed once with 1X PBS and were kept in Blocking Solution (0.1% Triton X-100, 2% BSA in 1X PBS) for 2h at room temperature. Blocking Solution was then replaced with the primary antibody diluted in Blocking Solution (100μL per coverslip) and incubated for 1h at room temperature. After 5 washes in Washing Solution (0.1% Triton X-100 in 1X PBS), 5 min at room temperature each, each coverslip was incubated with the secondary antibody diluted in 100μL of Blocking Solution for 1h at room temperature. Coverslips were then washed 5 times in Washing Solution for 5 min at room temperature, incubated with 1μg/mL DAPI in 1X PBS for 7 min at room temperature, washed twice in 1X PBS and mounted on glass slides with ProLong Diamond Antifade mountant (Invitrogen). Coverslips were sealed with nail polish the following day. Microscopy analysis was performed as described in the previous paragraph. The following primary antibody was used: rabbit polyclonal anti-RAP1 (NB100-292, Novus Biologicals; 1:500). The following secondary antibody was used: goat anti-rabbit-AF647 (1:1500; Invitrogen, A21245).

Immunofluorescence (IF)

Cells were fixed in 4% PFA for 20 min at room temperature, then washed twice with 1X PBS for 2 min at room temperature and then permeabilized with 0.5% Triton X-100 (in 1X PBS) for 5 min at room temperature. After three washes with 1X PBS, cells were kept in Blocking Solution (0.1% Triton X-100, 2% BSA in 1X PBS) for 2h at room temperature. From this step, samples were treated as indicated in the smiFISH/IF protocol. The following primary antibodies were used: rabbit polyclonal anti-RAP1 (NB100-292, Novus Biologicals; 1:500); mouse monoclonal anti-γH2AX (1:500; Millipore). The following secondary antibodies were used: goat anti-rabbit-AF555 (1:1500; Invitrogen, A21245); goat anti-mouse-AF488 (1:1500; Invitrogen).

Isolation of poly(A)$^+$ and poly(A)$^-$ RNA fractions

Total RNA was purified from HeLa, U2OS, HCT116 and MCF7 cells, treated with DNase I and its integrity was assessed by MOPS gel. 5 μg of RNA per sample were processed by Poly(A) RNA Selection Kit (Lexogen) following manufacturer's protocol. Poly(A)$^+$ RNA fraction was obtained by eluting the RNA bound to the oligo-dT resin. Poly(A)$^-$ RNA fraction was isolated by precipitating the RNA from washes using 1 volume of isopropanol for 30 min at −20°C in the presence of glycogen. Total RNA, poly(A)$^+$ and poly(A)$^-$ RNA fractions were reverse transcribed either with TERRA RT primers, for TERRA detection, or random hexamers, for *GAPDH*, *E2F1 and 18S rRNA* detection, using the Superscript III RT enzyme (Invitrogen). cDNA was analyzed by qPCR. The relative enrichment of transcripts was calculated as a percentage of total RNA and normalized over the poly(A).

Nuclear run-on (NRO)

The experiments were performed as described in Roberts et al., 2015,[49] with some modifications. Cells from 3 confluent plates of U2OS cells per condition were scraped and washed twice with ice-cold PBS. Nuclei were isolated resuspending cells in 10 mL ice-cold swelling buffer (Tris-HCL pH 7.5 10mM, MgCl2 2mM, CaCl2 3mM). After incubation on ice for 5 min and centrifugation at

400 g for 10 min, the supernatant was discarded and 10 mL of swelling buffer containing 10% glycerol supplemented with RNase inhibitor 2U/ml (RNase OUT Recombinant Ribonuclease Inhibitor Invitrogen) was added. 10 mL of lysis buffer (swelling buffer with glycerol, Igepal 1%) supplemented with RNase inhibitor 2U/ml was then added and samples were incubated for 5 min on ice. After adding 25 mL more of lysis buffer, samples were centrifuged, and the supernatant was discarded. Nuclei were resuspended in 10 mL freezing buffer (Tris-HCl pH 8 50mM, MgCl2 5mM, EDTA 0.1mM, glycerol 4%) supplemented with RNase inhibitor 2U/ml, centrifuged at 900 g for 6 min and supernatant was removed. Nuclei were resuspended in 90 μL freezing buffer and stored at −80°C overnight. Transcription was resumed *in vitro* in the presence of bromouridine with the addition of 90 μL 2X NRO buffer (10mM Tris-HCl pH 8, 5mM MgCl2, 300mM KCl, 1mM DTT, 500 μM ATP, 500 μM GTP, 500 μM Br-UTP (Santa Cruz Biotechnology), 2uM CTP, 200 U/ml RNase OUT, 1% N-Laurylsarcosine) and incubation at 30°C for 0, 10, 30 or 60 min 600 μL of TRIzol Reagent (Invitrogen) was added to each sample to block the reaction and nuclei were dissolved through vortexing after 5 min incubation at room temperature. 160 μL chloroform was added and the samples were shaken vigorously for 20 s and centrifuged at 12000 g for 30 min at 4°C. The upper clear aqueous phase, containing RNA, was transferred to new tubes, 1/10 vol NaAc 3M, 2 vol EtOH 100% and 1 μL glycogen (Invitrogen) were added and tubes were placed at −20°C overnight. RNA was precipitated by centrifugation at maximum speed for 30 min at 4°C. The supernatant was aspirated, and the pellet was washed with 75% ethanol and then dried under the hood. The dry pellet was then dissolved in 20 μL DEPC water. To immunoprecipitate bromouridine labeled RNA, 180 μL of binding buffer (0.25× SSPE, 0.05% Tween 20, 37.5 mM NaCl, 1mM EDTA) supplemented with RNase inhibitor 4 U/ml was added to the RNA samples. To each sample, 1 μg of monoclonal antibody anti-BrdU (Santa Cruz Biotechnology) was added, and the tubes were placed under rotation for 1h at room temperature. 20 μL of Protein G Dynabeads (Invitrogen) per sample was washed twice with blocking buffer (1× binding buffer with the addition of 0.1% polyvinylpyrrolidone and 0.1% BSA) and equilibrated in blocking buffer supplemented with RNase inhibitor for 1h at room temperature under rotation. Beads were then washed twice with binding buffer and added to the 200 μL of sample incubated with the antibody. Binding buffer was added to complete 700 μL of final volume to each sample. Samples were incubated for 1h at room temperature under rotation. After incubation, bead-bound RNAs were washed twice with binding buffer; twice with low salt buffer (0.2× SSPE, 0.05% Tween 20, 1mM EDTA), once with high salt buffer (0.2× SSPE, 137.5 mM NaCl, 0.05% Tween 20, 1mM EDTA) and twice with TE + tween buffer (0.01 M Tris, 0.001 M EDTA, pH 7.4, 0.05% Tween 20). The beads were resuspended in 100 μL elution buffer (50 mM Tris pH 7.5, 150 mM NaCl, 0.1% SDS, 20 mM DTT, 1 mM EDTA) and incubated 10 min at 37°C in a thermomixer at 900 rpm to elute RNA. The eluate was collected, and the elution was repeated 3 additional times. 1 mL EtOH 100%, 300mM NaCl and 1 μL glycogen were added to the 400 μL eluate, to precipitate RNA overnight at −20°C. After centrifugation at maximum speed for 30 min at 4°C, washing with 70% Ethanol and drying the pellet, RNA was resuspended in DEPC water for subsequent reverse transcription with oligo dT primer and quantification of polyadenylated TERRA, actin and GAPDH transcripts using specific qPCR primers.

Chromatin immunoprecipitation (ChIP)

HeLa cells were cultured on 10 cm Petri dishes to 70%–90% of confluence and crosslinked for 8 min with PBS containing 1% PFA (Electron Microscopy Science). Cells were then washed three times with 1X PBS and crosslinking was quenched by incubation in PBS containing 0.125 M glycine for 15 min. After three washes with 1X PBS, cells were collected and lysed by incubation in 1mL Solution A (10 mM HEPES pH 7.9, 1 mM EDTA pH 8, 0.5 mM EGTA, 0.25% Triton X-, supplemented with protease inhibitors) for 5 min at 4°C. After centrifugation at 1500 g at 4°C, nuclei pellets were incubated in 1mL Solution B (10 mM HEPES pH 7.9, 1 mM EDTA pH 8, 0.5 mM EGTA, 200 mM NaCl, supplemented with protease inhibitors) for 5 min at 4°C. After a second centrifugation at 1500 g at 4°C, pellets containing chromatin were resuspended in 1mL Solution C (50 mM HEPES pH 7.5, 150 mM NaCl, 0.1% deoxycholate, 1% SDS, 1% Triton X-, 40 μM PMSF, supplemented with protease inhibitors) for sonication using Bioruptor (Diagenode) in order to obtain 400-200 bp chromatin fragments. The size of the fragments was verified by running 10 μL of each sample in a 2% agarose gel. After sonication, samples were centrifuged at 14000 rpm for 15 min at 4°C. The supernatant was precleared for 2 h at 4°C with protein G magnetic beads (Invitrogen) and then lysates were incubated overnight at 4°C with either rabbit polyclonal anti-RALY antibody (3 μg; Bethyl), rabbit polyclonal anti-RAP1 antibody (3 μg; Novus Biologicals), or rabbit IgG polyclonal antibody (3 μg; Millipore). 20 μL of protein G magnetic beads were added to lysates and incubated for 2 h at 4°C. The beads were then washed four times for 10 min at 4°C: the first wash was performed in 0.5 mL of Buffer I (50 mM HEPES pH 7.5, 2 mM EDTA pH 8, 0.1% deoxycholate, 150 mM NaCl, 1% Triton X-, 1 mM DTT, supplemented with protease inhibitors); the second wash was performed in 0.5 mL of Buffer II (50 mM HEPES pH 7.5, 2 mM EDTA pH 8, 0.1% deoxycholate, 500 mM NaCl, 1% Triton X-, 1 mM DTT, supplemented with protease inhibitors); the third wash was performed in 0.5 mL of Buffer III (250 mM LiCl, 1 mM EDTA pH 8, 10 mM Tris-HCl pH 8, 0.5% NP-40, 1 mM DTT, supplemented with protease inhibitors); the fourth wash was performed in 0.5 mL TE Buffer (10 mM Tris-HCl pH 8, 1 mM EDTA pH 8, 1 mM DTT, supplemented with protease inhibitors). For validation experiments of protein immunoprecipitation, proteins were run on 10% SDS-PAGE for Western blot analysis. For DNA isolation and qPCR analyses, DNA was eluted from beads by incubation for 10 min at RT with Elution Buffer (0.5% SDS, 100 mM $NaHCO_3$), then RNase A (1:200, Macherey-Nagel) was added and incubated at 37°C for 30 min and finally Proteinase K (1:300, Thermo Scientific) was added and incubated at 55°C for 1 h. For decrosslinking, samples were incubated at 65°C overnight in 200 mM NaCl. DNA was isolated with Phenol/Chloroform/Isoamyl alcohol (25:24:1, Fisher BioReagents) according to manufacturer instructions using 0.3 mL of reagent per immunoprecipitated sample and input samples; DNA was then precipitated by NaAc and EtOH and the pellets resuspended in nuclease-free H_2O. DNA was then processed for DNA dot blot as described below.

RNaseH1-chromatin immunoprecipitation (R-ChIP)

R-ChIP experiments were performed following the ChIP procedure described above with the following differences: HeLa and U2OS clones expressing RNase H1 D210N were cultured on 10 cm Petri dishes. After sonication, rabbit monoclonal anti-V5 antibody (3 μg; Cell Signaling) was used to separate the RNaseH1-bound chromatin, or rabbit IgG polyclonal antibody (3 μg; Millipore) as control. For DNA isolation, DNA was eluted from antibody-bound magnetic beads (Thermo FIsher Scientific) by incubation for 10 min at RT with Elution Buffer (0.5% SDS, 100 mM $NaHCO_3$), and incubated with Proteinase K (1:300, Thermo Scientific) at 55°C for 1 h. After de-crosslinking, DNA extraction and precipitation, DNA samples were diluted for qPCR analyses. The relative enrichment of subtelomeric sequences was calculated according to the percentage of input.

DNA dot-blot

DNA from ChIP experiments was denatured in 1X SSC at 100°C for 10 min before blotting on an Amersham Hybond H+ membrane (GE Healthcare) using the BioDot apparatus (Bio-Rad), to obtain spots. After blotting, the membrane was incubated for 10 min in Denaturing solution (1.5 M NaCl, 500 mM NaOH) and then for 10 min in Neutralizing solution (3 M NaCl, 500 mM Tris-HCl pH 7). The membrane was then crosslinked with UV for 3 min at 120 mJ/cm^2 on the UVP CL-1000L Longwave Crosslinker (Fisher Scientific), pre-hybridized for 1 h in the UVP HB-1000 Hybridizer oven (Fisher Scientific) with pre-heated hybridization buffer (5X SSC, 0.1% sarkosyl, 0.04% SDS in H_2O) and hybridized with 5 nM telomeric or Alu 3′ DIG-labelled probes in hybridization buffer, overnight at 45°C for telomeric repeats detection, or at 48°C, for Alu repeats detection. Probe labeling was performed using DIG Oligonucleotide 3′ End-Labelling Kit (Roche) according to the manufacturer's protocol. After hybridization, the membrane was washed 2 times in 2X SSC/0.1% SDS for 5 min at RT, then 2 times in 0.5X SSC/0.1% SDS for 5 min at RT, 2 times in preheated 0.5X SSC/0.1% SDS for 15 min at 42°C and briefly in 2X SSC at RT. The membrane was incubated for 1 h at room temperature in blocking solution (Maleic acid buffer pH 7.5 (0.1M maleic acid, 0.15M sodium chloride) containing 1% Blocking Reagent (Roche) and for 30 min in blocking solution containing anti-DIG antibody (1:10000; Roche) at RT. Finally, the membrane was washed 2 times for 30 min in wash buffer (0.3% Tween 20, 0.5X Maleic Acid Buffer pH 7.5 in H_2O), equilibrated for 2 min in AP buffer (100mM Tris-HCl pH 9.5, 100mM NaCl in H_2O) and prepared for detection at the ChemiDoc XRS+ (Bio-Rad) with CDP-Star Chemiluminescence Substrate (Roche), according to the manufacturer's protocol.

QUANTIFICATION AND STATISTICAL ANALYSES

Details about the statistical analysis for each figure are provided in the figure legends. Significance is indicated as follows: *: $p < 0.05$, **: $p < 0.01$, ***: $p < 0.001$, ****: $p < 0.0001$, ns: not significant. GraphPad Prism 8 was used for statistical analyses. Excel was used for statistical analysis of actinomycin D experiment (Figures 2C and 2D).